A heuristic argument for the sole use of numerical stabilization with no physical LES modeling in the simulation of incompressible turbulent flows

Oriol Guasch[1] and Ramon Codina[2]

[1] Universitat Ramon Llull, C/Quatre Camins 2, 08022 Barcelona, Catalonia, Spain
[2] Universitat Politècnica de Catalunya, Jordi Girona 1-3, Edifici C1, 08034 Barcelona, Catalonia, Spain.

Contents

Abstract

We aim at giving support to the idea that no physical Large Eddy Simulation (LES) model should be used in the simulation of turbulent flows. It is heuristically shown that the rate of transfer of subgrid kinetic energy provided by the stabilization terms of the Orthogonal Subgrid Scale (OSS) finite element method is already proportional to the molecular physical dissipation rate (for an appropriate choice of the stabilization parameter). This precludes the necessity of including an extra LES physical model to achieve this behavior and somehow justifies the purely numerical approach to solve turbulent flows. The argumentation is valid for a fine enough mesh with characteristic element size, h, so that h lies in the inertial subrange of a turbulent flow.

Key Words: *Stabilized finite elements, Large Eddy Simulation, Variational Multiscale, Subgrid Scale modeling, Orthogonal Subgrid Scales, Turbulent flows*

1 Introduction

Two parallel lines have been followed in the past years to simulate incompressible turbulent flows that can be of engineering interest. On one side, the drawbacks of RANS (Reynolds Averaged Navier-Stokes) models combined with the impossibility to perform DNS (Direct Numerical Simulation) computations for large Reynolds number problems led to the development of LES (Large Eddy Simulation) strategies (see e.g., [43]). On the other side, the numerical problems that arise when trying to solve the discrete differential or weak versions of CDR (Convection-Diffusion-Reaction) equations have motivated the development of several stabilization strategies to mitigate them. A landmark in the development of these stabilization methods was the appearance of the *subgrid scale* stabilization approach or, as originally termed, the *variational multiscale* method (VMM), in the framework of finite element methods [27, 29]. Both approaches, LES and VMM applied to fluid dynamics, share some features like being based on a scale decomposition of the continuous velocity and pressure fields of the Navier-Stokes equations. However, in the former case this scale separation is performed at the continuous level while in the latter it is inherently carried out in the discretization process. The relation between both methods is not fully understood at present and it is not clear whether they should be used together or independently in the simulation of turbulent flows. In this paper we aim at giving some support to the idea that no LES physical model should be used if an appropriate discrete stabilization scheme is implemented.

In LES the scale decomposition between large and small flow scales has been traditionally performed by means of a filtering process (see e.g., [38, 17, 18]) defined through a convolution operation. The filter is applied to the Navier-Stokes equations usually assuming that it commutes with the differential operators and a new equation for the filtered velocity and pressure fields is derived. However, this equation contains the divergence of the so-called *residual stress* tensor that depends on the exact velocity field. This term has to be modeled somehow to obtain a closed system of equations only depending on filtered quantities. Once a physical LES model is chosen, the resulting filtered equation is finally discretized and solved.

This approach presents several mathematical difficulties such as knowing the error introduced when the commutation between the filtering and differentiation operators is assumed, knowing which should be the appropriate choice for the LES boundary conditions and, what is probably more important, knowing which is the relation between the errors introduced by the physical LES model and by the discretization procedure. Some of these subjects have received recent attention both from analytical (see e.g., [2, 34]) and numerical points of view (see e.g., [19, 5, 37, 35, 46]). In [23] a review of several LES models was performed and some interesting conclusions were drawn out, such as the fact that filtering is not indispensable to achieve LES models, that aiming at an exact closure for the residual

stress tensor is a paradoxic program and that some LES models have the remarkable propriety of being more regular than the original Navier-Stokes equations, leading to problems for which uniqueness of solutions can be proved. In this sense, it was concluded that a LES model should fulfill with two main requisites, namely, it should regularize the Navier-Stokes equations yielding to well-posed problems and it should lead to *suitable* weak solutions (i.e., physically acceptable solutions). In an attempt to provide a first step towards a mathematical definition of LES, the notion of *suitable approximations* to the Navier-Stokes equations was then introduced in [24]. In this context, it is worthwhile to mention that a DNS using the Galerkin method with low order finite elements constitutes a suitable approximation to the Navier-Stokes equations, which may justify the fact that sometimes better results are achieved for low-order methods when no LES model is employed [22].

In the VMM or subgrid scale approach to solve turbulent flows [30], the scale separation is carried out by means of a projection onto the finite element space. Two equations are then obtained respectively governing the dynamics of the large and small scales. Large scales are those that can be captured by the computational mesh, while small or subgrid scales are those not captured by the mesh. Modeling takes place when giving an approximated solution for the subgrid scales equation, which is to be inserted in the large scale equation to account for their effects.

The initial motivation of the VMM method was to solve some of the numerical problems associated with the simulation of the discrete Navier-Stokes equations, such as the necessity to satisfy the *inf-sup* condition (which implies the use of different interpolation spaces for the velocity and pressure fields) or the numerical instabilities appearing for convective dominated flows. Consequently, when the VMM was first applied to the simulation of turbulent flows a physical LES model (Smagorinsky model) was still included, although solely acting on the subgrid scale equation [30, 31, 32]. The idea that the stabilization terms in the VMM approach could be sufficient to simulate turbulent flows was already pointed out in the framework of orthogonal subgrid scale (OSS) stabilization methods [10] (see also [12]) as a natural extension to that work. Later it was re-introduced in [4, 33] and further elaborated in [28]. Recently, very good results have been obtained in the simulation of isotropic turbulence and turbulent channel flows with the sole use of numerical stabilization [1, 26, 44]. Actually, and as far as we know, this “numerical” line of thinking initiated with the MILES (Monotone Integrated LES) approach [3] c.f. [46] (see also [43] and references therein). We shall come back to this point in Section 5

In this paper a further argument supporting the non physical modeling approach will be given. An important point a closure LES model should satisfy is that the rate of kinetic energy transferred from the filtered large scales to the small ones should equal the physical dissipation rate at the Kolmogorov length scale (see e.g., [40, 42]). This is so for the filter width lying in the inertial subrange of the flow under study. Considering the OSS stabilized finite element method [8, 9, 10], it will be herein shown that the contribution to the energy balance equation from the stabilization terms that arise in the discrete weak Navier-Stokes from purely numerical considerations are in fact already proportional to the physical dissipation rate (for a fine enough computational mesh so that its characteristic element size lies in the inertial subrange of the considered turbulent flow). Consequently, the inclusion of an extra physical LES model seems somewhat redundant and unnecessary.

The paper is organized as follows. In section 2 the energy balance equations for the continuous Navier-Stokes and LES problems are presented together with their discrete counterparts using the Galerkin and OSS stabilized finite element methods. The problem we would like to address is established and the OSS stabilization terms accounting for the transfer of kinetic energy to subscales that should be proportional to the physical dissipation rate are identified. In section 3 we proceed to the explicit discretization of these terms, showing that their ensemble average can be written as products of geometrical factors multiplying two point second and fourth-order nodal velocity correlations, as well as triple-order velocity-pressure correlations. In section 4, results from fluid statistical mechanics are used to relate these correlations to the physical dissipation rate, which is the main goal of the pa-

per. Some general comments and remarks, together with references to recent numerical experiments supporting the pure numerical approach to solve turbulent flows are given in section 5. A numerical experiment of a turbulent flow impinging on a plate is also included. Conclusions are finally drawn in section 6.

2 Energy balance equations

2.1 Energy balance equation for the Navier-Stokes problem

The strong formulation of the Navier-Stokes equations problem consists in solving their differential version in a given domain $\Omega \subset \mathbb{R}^d$ (where $d = 2, 3$ is the number of space dimensions) with boundary $\partial\Omega$ and prescribed initial and boundary conditions. We will only consider homogeneous Dirichlet conditions on the boundary ($\partial\Omega \equiv \Gamma_D$) for simplicity and use the conservative form of the equations. Throughout the work we will concentrate on the three dimensional case ($d = 3$). The problem to be solved then reads

$$\partial_t \boldsymbol{u} - 2\nabla \cdot [\nu \boldsymbol{\mathcal{S}}(\boldsymbol{u})] + \nabla \cdot (\boldsymbol{u} \otimes \boldsymbol{u}) + \nabla p = \boldsymbol{f} \qquad \text{in } \Omega \times (0,T), \tag{1}$$

$$\nabla \cdot \boldsymbol{u} = 0 \qquad \text{in } \Omega \times (0,T), \tag{2}$$

$$\boldsymbol{u}(\boldsymbol{x},0) = \boldsymbol{u}_0(\boldsymbol{x}) \qquad \text{in } \Omega,\ t = 0, \tag{3}$$

$$\boldsymbol{u}(\boldsymbol{x},t) = 0 \qquad \text{on } \Gamma_D \times (0,T), \tag{4}$$

where $\boldsymbol{u}$ stands for the flow velocity, p for the pressure, ν represents the kinematic fluid viscosity (taken constant hereafter), $\boldsymbol{\mathcal{S}}(\boldsymbol{u}) := \frac{1}{2}\left(\nabla \boldsymbol{u} + \nabla \boldsymbol{u}^T\right)$ the rate of strain tensor, $\boldsymbol{f}$ the external force and $(0,T)$ is the time interval of analysis.

Use is made of the following notation to introduce the weak form associated to problem (1)-(4). $L^p(\Omega)$ denotes the spaces of functions whose p power $(1 \leq p < \infty)$ is integrable in Ω, with $p = \infty$ corresponding to the space of bounded functions in Ω. For $p = 2$ we have a Hilbert space with scalar product

$$(\boldsymbol{u}, \boldsymbol{v}) := \int_\Omega \boldsymbol{u}(\boldsymbol{x}) \boldsymbol{v}(\boldsymbol{x}) d\Omega \tag{5}$$

and induced norm $\|\boldsymbol{u}\|_{L^2(\Omega)} \equiv \|\boldsymbol{u}\| = (\boldsymbol{u}, \boldsymbol{u})^{1/2}$. From a physical point of view, $L^2(\Omega)$ can be identified with the space of velocity fields with bounded kinetic energy, given that $\|\boldsymbol{u}\|^2 = 2E(\boldsymbol{u})$, with $E(\boldsymbol{u})$ standing for the kinetic energy per unit mass.

$H^m(\Omega)$ denotes the space of functions whose distributional derivatives up to order m lay in $L^2(\Omega)$. The case $m = 1$ is of special interest as it is also a Hilbert space and can be physically identified with the space of velocity and vorticity fields having bounded energy and enstrophy [16]. On the other hand, $H_0^1(\Omega)$ stands for the functions in $H^1(\Omega)$ vanishing on Γ_D. $H^{-1}(\Omega)$ denotes the topological dual of $H_0^1(\Omega)$ and the brackets, $\langle \cdot, \cdot \rangle$, will be used for the duality pairing between these spaces. $\|\cdot\|_X$ designates the norm in a Banach space, X, and $L^p(0,T;X)$ is the space of time dependent functions such that their X-norm is $L^p(0,T)$. A bold character is used for the vector counterpart of all these spaces.

The weak form of problem (1)-(4) can be formulated as:
find $[\boldsymbol{u}, p] \in \boldsymbol{L}^2(0,T;\boldsymbol{H}_0^1(\Omega)) \times \mathcal{D}'(0,T;L^2(\Omega)/\mathbb{R})$ ($\mathcal{D}'$ being the space of distributions) such that

$$(\partial_t \boldsymbol{u}, \boldsymbol{v}) + 2\nu(\boldsymbol{\mathcal{S}}(\boldsymbol{u}), \boldsymbol{\mathcal{S}}(\boldsymbol{v})) + \langle \nabla \cdot (\boldsymbol{u} \otimes \boldsymbol{u}), \boldsymbol{v} \rangle - (p, \nabla \cdot \boldsymbol{v}) = \langle \boldsymbol{f}, \boldsymbol{v} \rangle, \tag{6}$$

$$(q, \nabla \cdot \boldsymbol{u}) = 0, \tag{7}$$

for all $[\boldsymbol{v}, q] \in \boldsymbol{H}_0^1(\Omega) \times L^2(\Omega)/\mathbb{R}$, and satisfying the initial condition in a weak sense.

For each $t \in (0,T)$, setting $\boldsymbol{v} = \boldsymbol{u}$, $q = ct$ (constant) in (6)-(7) (assuming this is allowed) and taking into account that we have limited the analysis to homogeneous Dirichlet boundary conditions, we obtain the energy balance equation

$$\frac{d}{dt}\left(\frac{1}{2}\left\|\boldsymbol{u}\right\|^2\right) = -2\nu\left\|\boldsymbol{\mathcal{S}}\left(\boldsymbol{u}\right)\right\|^2 + \langle \boldsymbol{f}, \boldsymbol{u}\rangle. \tag{8}$$

Equation (8) states that the time variation of the flow kinetic energy depends on two factors, namely, the molecular dissipation due to viscosity (which is clearly negative) and the power exerted by the external force that can be either positive or negative. Identifying the pointwise kinetic energy as $k := \boldsymbol{u}\cdot\boldsymbol{u}/2$, the pointwise molecular dissipation as $\varepsilon_{\mathrm{mol}} := 2\nu\left[\boldsymbol{\mathcal{S}}\left(\boldsymbol{u}\right) : \boldsymbol{\mathcal{S}}\left(\boldsymbol{u}\right)\right]$ and the pointwise power of the external force as $P_f := \boldsymbol{f}\cdot\boldsymbol{u}$ we can rewrite (8) as

$$\int_\Omega \frac{dk}{dt} d\Omega = -\int_\Omega \varepsilon_{\mathrm{mol}} d\Omega + \int_\Omega P_f d\Omega. \tag{9}$$

According to the Kolmogorov description of the energy cascade in turbulent flows [36] cf. [42], the flow can be viewed as driven by the external forces acting at the large scales (low wave numbers) and generating kinetic energy, which is transferred to the low scales (high wave numbers) by non-linear processes. When the Kolmogorov length is reached, the viscous dissipation, $\varepsilon_{\mathrm{mol}}$, in the r.h.s of (9) takes part transforming the flow kinetic energy into internal energy (heat is released).

2.2 Energy balance equation for a Large Eddy Simulation model

In the standard Large Eddy Simulation (LES) of turbulent flows, a scale separation between large and small scales for the velocity and pressure fields in the Navier-Stokes equations is carried out. As commented in the introduction, this has been done traditionally by means of a convolution of the latter fields with a low pass filter operator, $\overline{(\cdot)} : v \longmapsto \overline{v}$, so that the decomposition $[\boldsymbol{u}, p\,] = [\overline{\boldsymbol{u}}, \overline{p}\,] + [\boldsymbol{u}', p']$ is obtained (see e.g., [38] cf. [42], [43]). $[\overline{\boldsymbol{u}}, \overline{p}\,]$ stands for the large, filtered, scales while $[\boldsymbol{u}', p']$ represent the small, residual, scales.

Without getting into details on the type of filter used for the scale separation and assuming that the filtering operator commutes with differentiation (although this will be certainly a source of errors [47, 20, 15]), the following differential problem is obtained for the filtered velocity and pressure fields $[\overline{\boldsymbol{u}}, \overline{p}\,]$:

$$\partial_t \overline{\boldsymbol{u}} - 2\nabla\cdot\left[\nu\boldsymbol{\mathcal{S}}\left(\overline{\boldsymbol{u}}\right)\right] + \nabla\cdot\left(\overline{\boldsymbol{u}}\otimes\overline{\boldsymbol{u}}\right) + \nabla\overline{p} = \boldsymbol{f} - \nabla\cdot\boldsymbol{\mathcal{R}} \qquad \text{in } \Omega\times(0,T)\,, \tag{10}$$

$$\nabla\cdot\overline{\mathbf{u}} = 0 \qquad \text{in } \Omega\times(0,T)\,, \tag{11}$$

$$\overline{\boldsymbol{u}}\left(\boldsymbol{x},0\right) = \overline{\boldsymbol{u}}_0\left(\boldsymbol{x}\right) \qquad \text{in } \Omega,\ t=0, \tag{12}$$

$$\overline{\boldsymbol{u}}\left(\boldsymbol{x},t\right) = 0 \qquad \text{on } \Gamma_D\times(0,T)\,, \tag{13}$$

which is analogous to (1)-(4) except for the divergence of the tensor $\boldsymbol{\mathcal{R}}$ appearing in the r.h.s of (10). The tensor $\boldsymbol{\mathcal{R}} := \overline{\boldsymbol{u}\otimes\boldsymbol{u}} - \overline{\boldsymbol{u}}\otimes\overline{\boldsymbol{u}}$ is usually named the *residual stress tensor* or the *subgrid scale tensor* and an expression for it in terms of $\overline{\boldsymbol{u}}$ is needed to close the system of equations (10)-(13). The different models for $\boldsymbol{\mathcal{R}}$ give place to different LES models.

The weak formulation of problem (10)-(13) can be stated as: find $[\overline{\boldsymbol{u}}, \overline{p}] \in \boldsymbol{L}^2(0,T;\boldsymbol{H}^1_0(\Omega)) \times \mathcal{D}'(0,T;L^2(\Omega)/\mathbb{R})$ such that

$$\begin{aligned}\left(\partial_t\overline{\boldsymbol{u}},\boldsymbol{v}\right) + 2\nu\left(\boldsymbol{\mathcal{S}}\left(\overline{\boldsymbol{u}}\right),\boldsymbol{\mathcal{S}}\left(\boldsymbol{v}\right)\right) + \left\langle\nabla\cdot\left(\overline{\boldsymbol{u}}\otimes\overline{\boldsymbol{u}}\right),\boldsymbol{v}\right\rangle - \left(\overline{p},\nabla\cdot\boldsymbol{v}\right)& \\ = \left\langle\overline{\boldsymbol{f}},\boldsymbol{v}\right\rangle + \left\langle\boldsymbol{\mathcal{R}},\nabla\boldsymbol{v}\right\rangle\,,& \qquad (14)\\ \left(q,\nabla\cdot\overline{\boldsymbol{u}}\right) = 0,& \qquad (15)\end{aligned}$$

for all $[\boldsymbol{v}, q] \in \boldsymbol{H}_0^1(\Omega) \times L^2(\Omega)/\mathbb{R}$, and satisfying the initial condition in a weak sense. Taking into account that $\boldsymbol{\mathcal{R}}$ is symmetric, we can rewrite the second term in the r.h.s of (14) as $\langle \boldsymbol{\mathcal{R}}, \nabla \boldsymbol{v} \rangle = \langle \boldsymbol{\mathcal{R}}, \boldsymbol{\mathcal{S}}(\boldsymbol{v}) \rangle$. In addition, and without loss of generality, we will consider $\boldsymbol{\mathcal{R}}$ deviatoric, its volumetric part being absorbed in the pressure term.

Assuming again continuity in time, if we next set $\boldsymbol{v} = \overline{\boldsymbol{u}}$, $q = ct$, for each $t \in (0, T)$ in (14)-(15) we can obtain an energy balance for the filtered Navier-Stokes equations:

$$\frac{d}{dt}\left(\frac{1}{2}\left\|\overline{\boldsymbol{u}}\right\|^2\right) = -2\nu\left\|\boldsymbol{\mathcal{S}}(\overline{\boldsymbol{u}})\right\|^2 + \langle \boldsymbol{\mathcal{R}}, \boldsymbol{\mathcal{S}}(\overline{\boldsymbol{u}}) \rangle + \langle \overline{\boldsymbol{f}}, \overline{\boldsymbol{u}} \rangle. \tag{16}$$

We can now define the filtered pointwise kinetic energy $\overline{k} := \overline{\boldsymbol{u}} \cdot \overline{\boldsymbol{u}}/2$, the pointwise filtered molecular dissipation $\overline{\varepsilon}_{\mathrm{mol}} := 2\nu\left[\boldsymbol{\mathcal{S}}(\overline{\boldsymbol{u}}) : \boldsymbol{\mathcal{S}}(\overline{\boldsymbol{u}})\right]$, the rate of production of residual kinetic energy $\overline{\mathcal{P}}_r := -\boldsymbol{\mathcal{R}} : \boldsymbol{\mathcal{S}}(\overline{\boldsymbol{u}})$ and the pointwise power of the external filtered force $\overline{P}_f := \overline{\boldsymbol{f}} \cdot \overline{\boldsymbol{u}}$, so that we can rewrite (16) as

$$\frac{d}{dt}\int_\Omega \overline{k} d\Omega = -\int_\Omega \overline{\varepsilon}_{\mathrm{mol}} d\Omega - \int_\Omega \overline{\mathcal{P}}_r d\Omega + \int_\Omega \overline{P}_f d\Omega. \tag{17}$$

For a fully developed turbulent flow with the filter width in the inertial subrange, the filtered field accounts for almost all the kinetic energy of the flow. Thus, $\int_\Omega \overline{k} d\Omega \approx \int_\Omega k d\Omega$ and the first terms in (9) and (17) become nearly equal. If the external force mainly acts on the large scales of the flow, it will also happen that $\int_\Omega \overline{\mathcal{P}}_f d\Omega \approx \int_\Omega \mathcal{P}_f d\Omega$. On the other hand, the energy dissipated by the filtered field, $\overline{\varepsilon}_{\mathrm{mol}}$ is relatively small and can be neglected [42]. Consequently, comparing equation (17) with equation (9), we observe that in order for the LES model to behave correctly it should happen that $\int_\Omega \overline{\mathcal{P}}_r d\Omega \approx \int_\Omega \varepsilon_{\mathrm{mol}} d\Omega$. That is, the rate of production of residual kinetic energy should equal, in the mean, the energy dissipated by viscous processes at the very small scales (Kolmogorov length), which is the point of view expressed by Lilly [40].

In the case of some celebrated LES models, such as the Smagorinsky model [45], $\overline{\mathcal{P}}_r$ is always positive and there is no backscatter, i.e., the energy is always transferred from the filtered scales to the residual ones, but not vice versa. It is quite customary then to term $\overline{\mathcal{P}}_r$ as *subgrid* or *residual dissipation* and to denote it by $\varepsilon_{\mathrm{SGS}}$, see e.g., [46]. However, this may lead to confusion, especially when introducing the discrete stabilized numerical version of the original and filtered Navier-Stokes equations, so we will keep the notation $\overline{\mathcal{P}}_r$ in this work.

2.3 Energy balance equations in discrete problems: stabilized numerical approach of the original and filtered Navier-Stokes equations

2.3.1 Galerkin finite element approach

The Galerkin finite element approximation to problem (6)-(7) can be stated as: given the finite dimensional spaces $\mathcal{V}_{0,h}^d \subset \boldsymbol{H}_0^1(\Omega)$ and $\mathcal{Q}_{0,h} \subset L^2(\Omega)/\mathbb{R}$ find $[\boldsymbol{u}_h(t), p_h(t)] \in \boldsymbol{L}^2(0, T; \mathcal{V}_{0,h}^d) \times \mathcal{D}'(0, T; \mathcal{Q}_{0,h})$ such that

$$\begin{aligned}(\partial_t \boldsymbol{u}_h, \boldsymbol{v}_h) + 2\nu(\boldsymbol{\mathcal{S}}(\boldsymbol{u}_h), \boldsymbol{\mathcal{S}}(\boldsymbol{v}_h)) + \langle \nabla \cdot (\boldsymbol{u}_h \otimes \boldsymbol{u}_h), \boldsymbol{v}_h \rangle \\ -(p_h, \nabla \cdot \boldsymbol{v}_h) = \langle \boldsymbol{f}, \boldsymbol{v}_h \rangle, \qquad (18)\\ (q_h, \nabla \cdot \boldsymbol{u}_h) = 0, \qquad (19)\end{aligned}$$

for all $[\boldsymbol{v}_h, q_h] \in \mathcal{V}_{0,h}^d \times \mathcal{Q}_{0,h}$.

Note that equations (18)-(19) are still continuous in time. However, for the developments to be presented hereafter time discretization will be not required, so no explicit expression for it will be given. Anyway, and whatever time discrete scheme is used, it is well known that the Galerkin finite element

approach (18)-(19) presents several difficulties. On one hand, numerical instabilities are encountered when the non-linear convective term in the equation dominates the viscous one at high Reynolds number problems. On the other hand, a compatibility condition (*inf-sup* or *LBB* condition) is required to control the pressure term. This condition does not allow to use equal order interpolations to approximate the velocity and pressure fields. Further numerical instabilities are also found when small time steps are used, specially at the early stages of evolutionary processes.

Several stabilization strategies have been developed to circumvent the above numerical instabilities of the Galerkin finite element solution to the Navier-Stokes equations. We will concentrate here on the *subgrid scale* approach (also termed *variational multiscale method* or *residual-based stabilization*) originally developed by Hughes [27, 29] for the scalar convection-diffusion-reaction equation, and latter extended to other equations by many authors. In particular we will focus on the orthogonal subgrid scale (OSS) approach developed in [8, 9, 10, 12]. This will simplify some of the forthcoming analysis although the developments could be possibly extended to other methods.

2.3.2 Orthogonal subgrid scale stabilization

The subgrid scale finite element stabilization method applied to the present problem consists in first splitting the continuous spatial spaces where the solution is found as $\boldsymbol{H}_0^1(\Omega) = \mathcal{V}_{0,h}^d \oplus \tilde{\mathcal{V}}_0^d$ and $L^2(\Omega)/\mathbb{R} = \mathcal{Q}_{h,0} \oplus \tilde{\mathcal{Q}}_0$, with $\tilde{\mathcal{V}}_0^d$ and $\tilde{\mathcal{Q}}_0$ being any infinite dimensional spaces that respectively complete the finite element spaces $\mathcal{V}_{0,h}^d$ and $\mathcal{Q}_{h,0}$ in $\boldsymbol{H}_0^1(\Omega)$ and $L^2(\Omega)/\mathbb{R}$. The velocity and pressure fields can then be decomposed as $\boldsymbol{u} = \boldsymbol{u}_h + \tilde{\boldsymbol{u}}$ and $p = p_h + \tilde{p}$ (the same holds for the test functions $\boldsymbol{v} = \boldsymbol{v}_h + \tilde{\boldsymbol{v}}$, $q = q_h + \tilde{q}$).

The weak form of the Navier-Stokes equations can now be split into two systems of equations. This is done by first substituting $\boldsymbol{u} = \boldsymbol{u}_h + \tilde{\boldsymbol{u}}$ and $p = p_h + \tilde{p}$ in (6)-(7) and taking $[\boldsymbol{v}, q\,] = [\boldsymbol{v}_h, q_h\,]$, which corresponds to projecting (6)-(7) onto the finite element spaces. Then, a second equation is obtained by projecting (6)-(7) onto the finite element complementary spaces by setting $[\boldsymbol{v}, q\,] = [\tilde{\boldsymbol{v}}, \tilde{q}\,]$.

After integrating some terms by parts and neglecting terms involving integrals over interelement boundaries, the equation corresponding to the large scales (projection onto the finite element spaces) becomes [10, 12],

$$
\begin{aligned}
&(\partial_t \boldsymbol{u}_h, \boldsymbol{v}_h) + 2\nu(\boldsymbol{\mathcal{S}}\,(\boldsymbol{u}_h)\,, \boldsymbol{\mathcal{S}}\,(\boldsymbol{v}_h)) + \langle \nabla\cdot(\boldsymbol{u}_h \otimes \boldsymbol{u}_h)\,, \boldsymbol{v}_h\rangle \\
&\qquad - (p_h, \nabla\cdot\boldsymbol{v}_h) + (q_h, \nabla\cdot\boldsymbol{u}_h) \\
&\qquad - \sum_e \langle \tilde{\boldsymbol{u}}, 2\nu\nabla\cdot\boldsymbol{\mathcal{S}}\,(\boldsymbol{v}_h) + \nabla\cdot(\boldsymbol{u}_h\otimes\boldsymbol{v}_h) + \nabla q_h\rangle_{\Omega_e} \\
&\qquad + (\partial_t\tilde{\boldsymbol{u}}, \boldsymbol{v}_h) + \langle \nabla\cdot(\tilde{\boldsymbol{u}}\otimes\boldsymbol{u}_h)\,, \boldsymbol{v}_h\rangle \\
&\qquad + \langle \tilde{\boldsymbol{u}}\cdot\nabla\tilde{\boldsymbol{u}}, \boldsymbol{v}_h\rangle \\
&\qquad - (\tilde{p}, \nabla\cdot\boldsymbol{v}_h) = \langle \boldsymbol{f}, \boldsymbol{v}_h\rangle\,.
\end{aligned}
\tag{20}
$$

The first two lines of (20) contain the Galerkin terms previously found in (18)-(19). The third line includes terms that are already obtained in the stabilization of the linearized and stationary version of the Navier-Stokes equations [8, 9] (Oseen problem). These terms avoid the convection instabilities of the Galerkin formulation and also allow to use equal interpolations for the velocity and the pressure. The first term in the fourth line accounts for the time derivative of the subscales, while the second term provides global momentum conservation [12]. The term in the fifth line has a second order dependence on the velocity subscales and it is argued in [4] that has very little influence on the results. Consequently it will be neglected in what follows, which will simplify the analysis. Finally, the term in the sixth line accounts for the effects of the pressure subscales.

To solve (20) we need some expressions for the velocity and pressure subscales $[\tilde{\boldsymbol{u}}, \tilde{p}\,]$. These expressions can be found from the solution of the small subgrid scales equation (projection onto the finite element complementary spaces). Given that the latter equation cannot be solved exactly, an approximation for its solution is required. The different ways in how this approximated solution is obtained give place to different subgrid scale stabilization models. We will use here the orthogonal subgrid scale (OSS) approach, which is based on choosing the spaces orthogonal to the finite element ones as the complimentary spaces in the above formulation. Moreover *quasi-static* subscales will be considered, leading to the approximation [8, 9]:

$$\tilde{\boldsymbol{u}} \approx \tau_1 \boldsymbol{r}_{u,h}, \tag{21}$$

$$\tilde{p} \approx \tau_2 r_{p,h}, \tag{22}$$

where $\boldsymbol{r}_{u,h}$ and $r_{p,h}$ represent the orthogonal projection of the residuals of the finite element components $\boldsymbol{u}_h$ and p_h

$$\begin{aligned} \boldsymbol{r}_{u,h} &= -\Pi_h^{\perp}[\partial_t \boldsymbol{u}_h - 2\nu\nabla\cdot\boldsymbol{\mathcal{S}}\left(\boldsymbol{u}_h\right) + \nabla\cdot\left(\boldsymbol{u}_h\otimes\boldsymbol{u}_h\right) + \nabla p_h - \boldsymbol{f}] \\ &= -\Pi_h^{\perp}[-2\nu\nabla\cdot\boldsymbol{\mathcal{S}}\left(\boldsymbol{u}_h\right) + \nabla\cdot\left(\boldsymbol{u}_h\otimes\boldsymbol{u}_h\right) + \nabla p_h], \qquad (23) \\ r_{p,h} &= -\Pi_h^{\perp}[\nabla\cdot\boldsymbol{u}_h]. \qquad (24) \end{aligned}$$

$\Pi_h^{\perp}$ in the above equations stands for the orthogonal projection, $\Pi_h^{\perp} := I - \Pi_h$, with I being the identity and Π_h the L^2 projection onto the appropriate finite element space. In fact, the numerical analysis of the stationary and linearized problem is greatly simplified if this projection is weighted elementwise by the stabilization parameters, as shown in [11]. However, this is not essential for the following developments.

In the second line of (23) we have used precisely the fact that, once discretized, $\partial_t \boldsymbol{u}_h \subset \mathcal{V}_{0,h}^d$. We have also considered that the external force belongs to $\mathcal{V}_{0,h}^d$ i.e., it only acts at the large scales of the flow in accordance with the simplified vision of the energy cascade presented at the end of section 2.1. We have also introduced another simplification in the expressions for the velocity residual as only the finite element component has been considered in the advective velocity term. Note, in addition, that no implicit time dependence of the subscales has been considered (*quasi-static* approach). On the other hand, the viscous term in the above equations has to be evaluated elementwise.

The stabilization parameters appearing in (21)-(22) can be obtained from arguments based on a Fourier analysis for the subscales [10] that yield,

$$\tau_1 = \left[\left(c_1\frac{\nu}{h^2}\right)^2 + \left(c_2\frac{|\boldsymbol{u}_h|}{h}\right)^2\right]^{-1/2}, \tag{25}$$

$$\tau_2 = \frac{h^2}{c_1\tau_1}\,. \tag{26}$$

c_1 and c_2 in (25)-(26) are algorithmic parameters with recommended values of $c_1 = 4$ and $c_2 = 2$ for linear elements [7], while h stands for a characteristic mesh element size. Again, we have neglected the subscale contribution in the advective velocity of τ_1. The choice (25)-(26) for the stabilization parameters guarantees that the kinetic energy of the modeled subscales approximates the kinetic energy of the exact subscales [10]. In the forthcoming analysis we will consider τ_1 and τ_2 constant within each element and typified by a characteristic element velocity to be defined later on.

Equation (20) together with the approximation (21)-(22) for the subscales constitute the proposed numerical approach to solve the incompressible Navier-Stokes equations. It will be argued that this scheme should also be valid for the simulation of turbulent flows without the necessity to perform a LES scale separation at the continuous level, prior to the numerical discretization.

2.3.3 Energy balance for the orthogonal subgrid scale finite element approach to the Navier-Stokes problem

In order to find an energy balance equation for the OSS numerical approach to the Navier-Stokes equations we can now set $\boldsymbol{v}_h = \boldsymbol{u}_h$ and $q_h = ct$ in (20). This yields (no approximation for the subscales is considered for the moment)

$$\begin{aligned}
&\frac{1}{2}\frac{d}{dt}\left\|\boldsymbol{u}_h\right\|^2 = -2\nu\left\|\boldsymbol{\mathcal{S}}\left(\boldsymbol{u}_h\right)\right\|^2 \\
&-\sum_e \langle \tilde{\boldsymbol{u}}, 2\nu\boldsymbol{\mathcal{S}}\left(\boldsymbol{u}_h\right) + \nabla\cdot\left(\boldsymbol{u}_h\otimes\boldsymbol{u}_h\right)\rangle_{\Omega_e} + \sum_e \left(\tilde{p}, \nabla\cdot\boldsymbol{u}_h\right)_{\Omega_e} + \langle \boldsymbol{f}, \boldsymbol{u}_h\rangle,
\end{aligned} \tag{27}$$

where Ω_e denotes the domain of the e-th element. Here and below, the summations with index e are assumed to be extended over all the elements.

If we now consider the subscales approximation (21)-(24) in (27) we obtain

$$\begin{aligned}
&\frac{1}{2}\frac{d}{dt}\left\|\boldsymbol{u}_h\right\|^2 = -2\nu\left\|\boldsymbol{\mathcal{S}}\left(\boldsymbol{u}_h\right)\right\|^2 + \langle \boldsymbol{f}_h, \boldsymbol{u}_h\rangle \\
&-\sum_e \tau_1\big(\Pi_h^{\perp}\big[-2\nu\nabla\cdot\boldsymbol{\mathcal{S}}\left(\boldsymbol{u}_h\right) + \nabla\cdot\left(\boldsymbol{u}_h\otimes\boldsymbol{u}_h\right) + \nabla p_h\big], \\
&2\nu\nabla\cdot\boldsymbol{\mathcal{S}}\left(\boldsymbol{u}_h\right) + \nabla\cdot\left(\boldsymbol{u}_h\otimes\boldsymbol{u}_h\right)\big)_{\Omega_e} - \sum_e \tau_2\left(\Pi_h^{\perp}\left(\nabla\cdot\boldsymbol{u}_h\right), \nabla\cdot\boldsymbol{u}_h\right)_{\Omega_e}.
\end{aligned} \tag{28}$$

Since we are interested in high Reynolds numbers, all the stabilization terms multiplied by the viscosity will be neglected, from where we obtain the following energy balance equation for the OSS stabilized finite element approach to the Navier-Stokes equations:

$$\begin{aligned}
&\frac{1}{2}\frac{d}{dt}\left\|\boldsymbol{u}_h\right\|^2 = -2\nu\left\|\boldsymbol{\mathcal{S}}\left(\boldsymbol{u}_h\right)\right\|^2 + \langle \boldsymbol{f}_h, \boldsymbol{u}_h\rangle \\
&-\sum_e \tau_1\left(\Pi_h^{\perp}\left[\nabla\cdot\left(\boldsymbol{u}_h\otimes\boldsymbol{u}_h\right) + \nabla p_h\right], \nabla\cdot\left(\boldsymbol{u}_h\otimes\boldsymbol{u}_h\right)\right)_{\Omega_e} \\
&-\sum_e \tau_2\left(\Pi_h^{\perp}\left(\nabla\cdot\boldsymbol{u}_h\right), \nabla\cdot\boldsymbol{u}_h\right)_{\Omega_e}.
\end{aligned} \tag{29}$$

Let us define the pointwise numerical kinetic energy of the flow as $k^h := \frac{1}{2}\left|\boldsymbol{u}_h\right|^2$, the pointwise molecular numerical dissipation for the large scales as $\varepsilon^h_{\mathrm{mol}} := 2\nu\boldsymbol{\mathcal{S}}\left(\boldsymbol{u}_h\right) : \boldsymbol{\mathcal{S}}\left(\boldsymbol{u}_h\right)$ and the pointwise numerical power for the external force as $P^h_f := \boldsymbol{f}_h\cdot\boldsymbol{u}_h$. We will also identify $\mathcal{P}^{h\tau}_r$ within each element with

$$\mathcal{P}^{h\tau}_r := \tau_1\mathcal{P}^{h\tau_1}_r + \tau_2\mathcal{P}^{h\tau_2}_r \tag{30}$$

where

$$\mathcal{P}^{h\tau_1}_r := \Pi_h^{\perp}\left[\nabla\cdot\left(\boldsymbol{u}_h\otimes\boldsymbol{u}_h\right) + \nabla p_h\right]\cdot\left[\nabla\cdot\left(\boldsymbol{u}_h\otimes\boldsymbol{u}_h\right)\right] \tag{31}$$

$$\mathcal{P}^{h\tau_2}_r := \Pi_h^{\perp}\left(\nabla\cdot\boldsymbol{u}_h\right)\left(\nabla\cdot\boldsymbol{u}_h\right). \tag{32}$$

Equipped with these definitions, equation (29) can be rewritten as

$$\frac{d}{dt}\int_\Omega k^h d\Omega = -\int_\Omega \varepsilon^h_{\mathrm{mol}} d\Omega - \sum_e \int_{\Omega_e} \mathcal{P}^{h\tau}_r d\Omega_e + \int_\Omega P^h_f d\Omega\,, \tag{33}$$

which can be compared with the energy balance equation of the continuous problem (9), using similar arguments to those in section 2.2.

It is clear that k^h will account for nearly the whole pointwise kinetic energy of the flow so that $\int_\Omega k^h d\Omega \approx \int_\Omega k d\Omega$. On the other hand, it will also occur that $\int_\Omega P_f^h d\Omega \approx \int_\Omega P_f d\Omega$, given that the force only acts at the large scales. In addition the numerical molecular dissipation of the large scales will be negligible, so that $\int_\Omega \varepsilon_{\rm mol}^h d\Omega \approx 0$.

The next, crucial, question is if it should happen that $\sum_e \int_{\Omega_e} \mathcal{P}_r^{h\tau} d\Omega \approx \int_\Omega \varepsilon_{\rm mol} d\Omega$ for the OSS formulation to be a good numerical approach for the Navier-Stokes equations, in the case of fully developed turbulence. Actually, this should not be necessarily the case for all the terms in $\mathcal{P}_r^{h\tau}$, given that they have arisen in the equation motivated by pure numerical stabilization necessities. However, it is clear that at least some of these terms should account for the appropriate physical behavior and their domain integration should approximate the mean molecular dissipation in (9). It will be the main result of this work to show, by means of heuristic reasoning, that actually the whole $\mathcal{P}_r^{h\tau}$ satisfies this assumption. It should be also noted that in the definition of $\mathcal{P}_r^{h\tau}$, the approximation for high Reynolds number flows was already performed (stabilization terms multiplied by the viscosity have been neglected).

2.3.4 Energy balance for the orthogonal subgrid scale finite element approach to a LES model

We could now proceed to discretize the LES equations (14)-(15) using the OSS approach. The usual way to do so is by simply adding the Navier-Stokes stabilization terms to the Galerkin discretization of the LES equations, i.e., terms containing the residual stress tensor, $\boldsymbol{\mathcal{R}}$, are not included in the stabilization terms (see e.g., [46]). This approach is in fact non consistent unless linear elements are used. However, in the OSS method this approach still makes sense given that the consistency error becomes optimal (see [11]).

The following discrete energy balance equation for the LES model analogous to (33) is obtained

$$\int_\Omega \frac{d\overline{k}^h}{dt} d\Omega = -\int_\Omega \overline{\varepsilon}_{\rm mol}^h d\Omega - \sum_e \int_{\Omega_e} \overline{\mathcal{P}}_r^{h\tau} d\Omega - \int_\Omega \overline{\mathcal{P}}_r^h d\Omega + \int_\Omega \overline{P}_f^h d\Omega \,, \tag{34}$$

with $k^h := \frac{1}{2}|\overline{\boldsymbol{u}}_h|^2$, $\overline{\varepsilon}_{\rm mol}^h := 2\nu \boldsymbol{S}(\overline{\boldsymbol{u}}_h) : \boldsymbol{S}(\overline{\boldsymbol{u}}_h)$, $\overline{P}_f^h := \overline{\boldsymbol{f}}_h \cdot \overline{\boldsymbol{u}}_h$, $\overline{\mathcal{P}}_r^h := -\boldsymbol{\mathcal{R}} : \boldsymbol{\mathcal{S}}(\overline{\boldsymbol{u}}_h)$ and $\overline{\mathcal{P}}_r^{h\tau} := -\sum_e \tau_1 (\Pi_h^\perp [\nabla \cdot (\overline{\boldsymbol{u}}_h \otimes \overline{\boldsymbol{u}}_h) + \nabla \overline{p}_h], \Pi_h^\perp [\nabla \cdot (\overline{\boldsymbol{u}}_h \otimes \overline{\boldsymbol{u}}_h)])_{\Omega_e} - \sum_e \tau_2 (\Pi_h^\perp (\nabla \cdot \overline{\boldsymbol{u}}_h), \Pi_h^\perp (\nabla \cdot \overline{\boldsymbol{u}}_h))_{\Omega_e}$. Following the argumentation lines in the above sections it is clear that the kinetic energy term will approximate the one in the exact energy balance equation (9). The same will prove true for the external force power and, again, $\overline{\varepsilon}_{\rm mol}^h$ will be negligible. However, we are now left with the curious fact that the two terms involving $\overline{\mathcal{P}}_r^{h\tau}$ and $\overline{\mathcal{P}}_r^h$ should equal, in the mean, the molecular physical dissipation. This seems at least redundant if the term containing $\overline{\mathcal{P}}_r^{h\tau}$ that arises from the discretization of the original Navier-Stokes equation already presents this behavior. In other words, the process of first filtering at the continuum level, modeling, and then proceeding to discretization (LES method) looks unnecessary if an appropriate numerical discretization scheme is used. Obviously, for an inaccurate discretization scheme the addition of extra dissipation as that provided by LES may be useful, but this should not be the case. In the following sections we aim at giving support to this idea by means of some heuristic reasoning.

3 Numerical subgrid kinetic energy transfer for high Reynolds numbers using the OSS stabilized FEM

3.1 Elemental ensemble average of $\mathcal{P}_r^{h\tau}$ for high Reynolds numbers

3.1.1 Stabilization parameters at high Reynolds numbers

In (25) an expression is given for the stabilization parameter τ_1. In the case of high Reynolds number flows the viscosity term in this expression can be discarded in front of the convective one, yielding

$$\tau_1 \approx \frac{h}{c_2 \left| \boldsymbol{u}_h \right|} \ . \tag{35}$$

On the other hand, using (35) in the expression for the parameter τ_2 in (26) we get

$$\tau_2 \approx \frac{c_2}{c_1} h \left| \boldsymbol{u}_h \right| \ . \tag{36}$$

When using the above stabilization parameters in a finite element implementation, h represents a characteristic element length of Ω_e, while $\boldsymbol{u}_h$ stands for a characteristic velocity at each element of the partition. Several options exist for the latter giving place to different OSS stabilization methods. One could take for example the velocity mean value at the element or its root mean square value. Whatever choice is made the key point for the forthcoming results is that τ_1 should depend inversely on this characteristic velocity while τ_2 should be proportional to it. This behavior will allow us to relate $\mathcal{P}_r^{h\tau}$ with the molecular dissipation rate $\varepsilon_{\rm mol}$, a fact that can be inversely be viewed as a confirmation of the right choice for τ_1 and τ_2 in (35)-(36).

As mentioned in the introduction, for a given computational mesh we will consider the case of the characteristic element size h being fine enough so as to lay in the inertial subrange. The inertial subrange can be thought as having limiting values $[l_{DI}, l_{EI}]$ with $l_{DI} \approx 60\eta$ and $l_{EI} \approx L/6$. η represents the Kolmogorov length where dissipation takes place and L corresponds to the flow scale typical of the largest, anisotropic eddies (see e.g., [42]). Let us denote by U the ensemble average (or time average under the ergodic assumption) of the chosen characteristic velocity at a given mesh element, to be used in the expressions for the stabilization parameters. Kolomogorov's second similarity hypothesis then guarantees that for an eddy of size ℓ, such that $\ell \in [l_{DI}, l_{EI}]$, U can only depend on $\varepsilon_{\rm mol}$ and ℓ, actually $U \sim (\varepsilon_{\rm mol}\ell)^{1/3}$. Our assumptions on the mesh discretization imply that $\ell \geq Ch$, with $C > 1$ a dimensionless constant. It then follows that the elemental stabilization parameters become

$$\tau_{1,ae} \sim \frac{h}{U} \sim \frac{h}{(\varepsilon_{\rm mol}\ell)^{1/3}} \, , \tag{37}$$

$$\tau_{2,ae} \sim hU \sim h\,(\varepsilon_{\rm mol}\ell)^{1/3} \ , \tag{38}$$

where all constants have been included inside U. The symbol $\sim$ is used here to denote *behaves as*, that is, the terms related by this symbol are approximately equal up to constants. However, we will abuse of language and in what follows the equality sign will be frequently employed in expressions containing approximated terms of the type (37)-(38).

3.1.2 Elemental ensemble average of $\mathcal{P}_r^{h\tau_1}$

Let us denote by $\Pi_i^h\left[\nabla\cdot(\boldsymbol{u}_h\otimes\boldsymbol{u}_h)+\nabla p_h\right]$ the i-th component of the projector in the definition of the numerical subgrid kinetic energy transfer term $\mathcal{P}_r^{h\tau_1}$ in (31) and denote the i-th velocity component by u_{hi}.

We consider a finite element partition of the domain Ω having n_p pressure nodes, n_u velocity nodes and n_e elements. Following similar lines of what is done in [13] (although with a very different objective) we define the average value in a mesh element Ω_e of $\mathcal{P}_r^{h\tau_1}$ in (31) as

$$\begin{aligned}\mathcal{P}_{r,e}^{h\tau_1} &= \frac{1}{V_e}\int_{\Omega_e}\left(\mathcal{P}_r^{h\tau_1}\right)d\Omega_e \\ &= \frac{1}{V_e}\int_{\Omega_e}\Pi_i^{h,\perp}\big[\nabla\cdot(\boldsymbol{u}_h\otimes\boldsymbol{u}_h)+\nabla p_h\big]\cdot\big[\nabla\cdot(\boldsymbol{u}_h\otimes\boldsymbol{u}_h)\big]d\Omega_e. \end{aligned} \tag{39}$$

An ensemble average (or time average under the ergodic assumption) of this quantity can be performed to obtain

$$\left\langle\mathcal{P}_{r,e}^{h\tau_1}\right\rangle = \frac{1}{V_e}\left\langle\int_{\Omega_e}\Pi_i^{h,\perp}\big[\nabla\cdot(\boldsymbol{u}_h\otimes\boldsymbol{u}_h)+\nabla p_h\big]\cdot\big[\nabla\cdot(\boldsymbol{u}_h\otimes\boldsymbol{u}_h)\big]d\Omega_e\right\rangle \tag{40}$$

(Brackets are used in this section to denote ensemble average instead of duality pairing). We next identify the terms $\left\langle\mathcal{P}_{r,e}^{h\tau_1}\right\rangle_U$ and $\left\langle\mathcal{P}_{r,e}^{h\tau_1}\right\rangle_P$ in (40) that will be treated independently in the analysis. We have

$$\begin{aligned}\left\langle\mathcal{P}_{r,e}^{h\tau_1}\right\rangle_U &:= \frac{1}{V_e}\left\langle\int_{\Omega_e}\Pi_i^{h,\perp}\big[\nabla\cdot(\boldsymbol{u}_h\otimes\boldsymbol{u}_h)\big]\cdot\big[\nabla\cdot(\boldsymbol{u}_h\otimes\boldsymbol{u}_h)\big]d\Omega_e\right\rangle \\ &= \frac{1}{V_e}\left\langle\int_{\Omega_e}\partial_i\left(u_{hi}u_{hj}\right)\partial_k\left(u_{hk}u_{hj}\right)d\Omega_e\right\rangle \\ &\quad-\frac{1}{V_e}\left\langle\int_{\Omega_e}\Pi_i^h\big[\nabla\cdot(\boldsymbol{u}_h\otimes\boldsymbol{u}_h)\big]\partial_j\left(u_{hj}u_{hi}\right)d\Omega_e\right\rangle \end{aligned} \tag{41}$$

and

$$\begin{aligned}\left\langle\mathcal{P}_{r,e}^{h\tau_1}\right\rangle_P &:= \frac{1}{V_e}\left\langle\int_{\Omega_e}\Pi_i^{h,\perp}\big(\nabla p_h\big)\cdot\big[\nabla\cdot(\boldsymbol{u}_h\otimes\boldsymbol{u}_h)\big]d\Omega_e\right\rangle \\ &= \frac{1}{V_e}\left\langle\int_{\Omega_e}\partial_i p_h\partial_j\left(u_{hj}u_{hi}\right)d\Omega_e\right\rangle \\ &\quad-\frac{1}{V_e}\left\langle\int_{\Omega_e}\Pi_i^h\big(\nabla p_h\big)\partial_j\left(u_{hj}u_{hi}\right)d\Omega_e\right\rangle, \end{aligned} \tag{42}$$

Above and in the following, summation is understood over spatial repeated indexes.

Obviously, we have

$$\left\langle\mathcal{P}_{r,e}^{h\tau_1}\right\rangle = \left\langle\mathcal{P}_{r,e}^{h\tau_1}\right\rangle_U + \left\langle\mathcal{P}_{r,e}^{h\tau_1}\right\rangle_P. \tag{43}$$

3.1.3 Elemental ensemble average of $\mathcal{P}_r^{h\tau_2}$

Proceeding analogously to what has been done in the previous section but for the $\mathcal{P}_r^{h\tau_2}$ term defined in (32), it can readily be checked that the elemental ensemble average of $\mathcal{P}_r^{h\tau_2}$ becomes

$$\begin{aligned}\left\langle\mathcal{P}_{r,e}^{h\tau_2}\right\rangle &:= \frac{1}{V_e}\left\langle\int_{\Omega_e}\Pi^{h,\perp}\big(\nabla\cdot\boldsymbol{u}_h\big)\big(\nabla\cdot\boldsymbol{u}_h\big)d\Omega_e\right\rangle \\ &= \frac{1}{V_e}\left\langle\int_{\Omega_e}\left(\partial_i u_{hi}\right)^2 d\Omega_e\right\rangle - \frac{1}{V_e}\left\langle\int_{\Omega_e}\Pi^h\big(\nabla\cdot\boldsymbol{u}_h\big)\left(\partial_i u_{hi}\right)d\Omega_e\right\rangle. \end{aligned} \tag{44}$$

3.1.4 Elemental ensemble average of $\mathcal{P}_r^{h\tau}$

From (30) and using the elemental stabilization parameters (37)-(38) as well as (40) and (44), we can define the ensemble average of the rate of production of kinetic energy $\mathcal{P}_r^{h\tau}$ for high Reynolds numbers as

$$\left\langle \mathcal{P}_{r,e}^{h\tau} \right\rangle := \tau_{1,ae} \left\langle \mathcal{P}_{r,e}^{h\tau_1} \right\rangle + \tau_{2,ae} \left\langle \mathcal{P}_{r,e}^{h\tau_2} \right\rangle . \tag{45}$$

3.2 FEM solution and treatment of the L^2 projection in $\left\langle \mathcal{P}_{r,e}^{h\tau} \right\rangle$

3.2.1 FEM solution for the velocity and pressure fields and L^2 projection

The components of the discrete velocity field $\boldsymbol{u}_h$ can be expanded as usual for a mesh having n_u nodes as

$$u_{hi}\left(\boldsymbol{x}\right) = \sum_{a=1}^{n_u} N_u^a\left(\boldsymbol{x}\right) U_i^a, \tag{46}$$

where the velocity shape functions $\{N_u^a\left(\boldsymbol{x}\right), a = 1, \ldots, n_u\}$ are a basis of $\mathcal{V}_{0,h}^d$ and U_i^a are the velocity nodal values, i.e., at the nodal points, $\boldsymbol{x}^b$, $b = 1, \ldots, n_u$, it holds that

$$u_{hi}(\boldsymbol{x}^b) = U_i^b. \tag{47}$$

In case of $\boldsymbol{u}_h$ being the finite element interpolant, the nodal values are exact and

$$u_{hi}(\boldsymbol{x}^b) = U_i^b = u_i(\boldsymbol{x}^b) \equiv u_i^b. \tag{48}$$

Let us also assume the following interpolation for the Reynolds stresses (see e.g., [6])

$$u_{hi}u_{hj}\left(\boldsymbol{x}\right) = \sum_{b=1}^{n_u} N_u^b\left(\boldsymbol{x}\right) U_i^b U_j^b \tag{49}$$

in order to have simpler expressions and to make some of the forthcoming results useful from a computational point of view.

Concerning the discrete pressure field, p_h, it will be expanded as

$$p_h\left(\boldsymbol{x}\right) = \sum_{a=1}^{n_p} N_p^a\left(\boldsymbol{x}\right) P^a, \tag{50}$$

where the pressure shape functions $\left\{N_p^a\left(\boldsymbol{x}\right), a = 1, \ldots, n_p\right\}$ are a basis of $\mathcal{Q}_{h,0}$ and P^a denotes the pressure nodal value at node $\boldsymbol{x}^a$. We note that one of the advantages of using a stabilized finite element method such as the OSS in section 2.3.2 is that one can choose $N_u^a = N_p^a \equiv N^a$, hence circumventing the necessity of using different interpolations for the velocity and pressure fields as demanded by the *inf-sup* condition (see. e.g. [27, 29, 8, 9, 10]).

On the other hand, it will be necessary to give explicit expressions for the projected terms $\Pi_i^h\left[\nabla \cdot \left(\boldsymbol{u}_h \otimes \boldsymbol{u}_h\right)\right]$ and $\Pi_i^h\left(\nabla p_h\right)$ appearing in (41), (42) and (44). This can be done as follows. Consider a function ψ_h computed from the finite element interpolation, not necessarily continuous. Its L^2 projection onto $\mathcal{V}_{0,h}^d$ can be written as

$$\Pi(\psi_h) = \sum_{a=1}^{n_u} N^a\left(\boldsymbol{x}\right) \Pi^a, \tag{51}$$

with the coefficients Π^a being given by the solution of the linear system

$$\sum_{a=1}^{n_u} M^{ba}\Pi^a = \int_\Omega N^b \psi_h d\Omega, \quad b = 1, \ldots, n_u \tag{52}$$

$$M^{ba} := \int_\Omega N^b N^a d\Omega. \tag{53}$$

The mass matrix $\boldsymbol{M}$ in (53) can be approximated by means of a diagonal matrix of the form $\mathrm{diag}(\mathcal{M}_{11}, \ldots, \mathcal{M}_{n_u n_u})$ using a standard nodal quadrature rule. In this case

$$\Pi^b = \mathcal{M}_{bb}^{-1} \int_\Omega N^b \psi_h d\Omega, \tag{54}$$

so (53) becomes

$$\Pi(\psi_h) = \sum_{a=1}^{n_u} \mathcal{M}_{aa}^{-1} N^a \int_\Omega N^a \psi_h d\Omega\,. \tag{55}$$

3.2.2 $\left\langle \mathcal{P}_{r,e}^{h\tau} \right\rangle$ in terms of the finite element velocity and pressure fields

We next have to substitute the above expansions for the discrete velocity and pressure fields in the expressions for $\left\langle \mathcal{P}_{r,e}^{h\tau_1} \right\rangle_U$, $\left\langle \mathcal{P}_{r,e}^{h\tau_1} \right\rangle_P$ and $\left\langle \mathcal{P}_{r,e}^{h\tau_2} \right\rangle$, respectively given by equations (41), (42) and (44).

Convective term $\left\langle \mathcal{P}_{r,e}^{h\tau_1} \right\rangle_U$ corresponding to the velocity subscales (41). We will first address the term in the second line of (41), which will be denoted by $\left\langle \mathcal{P}_{r,e}^{h\tau_1} \right\rangle_{U,1}$. Substituting (49) in this term yields

$$\begin{aligned}\left\langle \mathcal{P}_{r,e}^{h\tau 1} \right\rangle_{U,1} &= \frac{1}{V_e}\left\langle \int_{\Omega_e} \left[\sum_a \partial_i N^a U_i^a U_j^a \sum_b \partial_k N^b U_k^b U_j^b \right] d\Omega_e \right\rangle \\ &= \frac{1}{V_e}\left[\sum_{a,b} \left\langle U_i^a U_j^a U_k^b U_j^b \right\rangle \int_{\Omega_e} \partial_i N^a \partial_k N^b d\Omega_e \right].\end{aligned} \tag{56}$$

The term in the third line of (41) will be denoted by $\left\langle \mathcal{P}_{r,e}^{h\tau_1} \right\rangle_{U,2}$. After substituting (49) and (55) in it, we get

$$\begin{aligned}\left\langle \mathcal{P}_{r,e}^{h\tau_1} \right\rangle_{U,2} &= -\frac{1}{V_e}\left\langle \int_{\Omega_e} \left[\sum_{a,c} \mathcal{M}_{cc}^{-1} N^c \int_\Omega N^c \partial_i N^a U_i^a U_j^a d\Omega \sum_b \partial_k N^b U_k^b U_j^b \right] d\Omega_e \right\rangle \\ &= -\frac{1}{V_e}\left\{ \sum_{a,b} \left\langle U_i^a U_j^a U_k^b U_j^b \right\rangle \int_{\Omega_e} \left[\partial_k N^b \sum_c \mathcal{M}_{cc}^{-1} N^c \int_\Omega N^c \partial_i N^a d\Omega \right] d\Omega_e \right\}.\end{aligned} \tag{57}$$

To facilitate the notation in expressions (56) and (57) we define the geometric factors

$$I_{ij}^{ab} := \int_{\Omega_e} \partial_j N^b \partial_i N^a d\Omega_e \tag{58}$$

and

$$G_{ij}^{ab} := \int_{\Omega_e} \left[\partial_j N^b \sum_c \mathcal{M}_{cc}^{-1} N^c \int_\Omega N^c \partial_i N^a d\Omega \right] d\Omega_e. \tag{59}$$

Both factors depend on the element Ω_e. However, while I_{ij}^{ab} has a *local* character in the sense that it only depends on the shape functions and the type of element being used, G_{ij}^{ab} has a *global* character

because it involves an integration over the whole computational domain Ω. This global character is due to the fact that a projection is involved in $\left\langle \mathcal{P}^{h\tau_1}_{r,e} \right\rangle_{U,2}$.

We will also denote the velocity correlation function as

$$B^{ab}_{ij} = \left\langle U^a_i U^b_j \right\rangle. \tag{60}$$

and the two point fourth moment of the velocity field by

$$B^{ab}_{ij,kl} = \left\langle U^a_i U^a_j U^b_k U^b_l \right\rangle. \tag{61}$$

Using the notation (58)-(61) in equations (56) and (57), we obtain the following expansion for the convective term $\left\langle \mathcal{P}^{h\tau_1}_{r,e} \right\rangle_U$:

$$\left\langle \mathcal{P}^{h\tau_1}_{r,e} \right\rangle_U = \left\langle \mathcal{P}^{h\tau_1}_{r,e} \right\rangle_{U,1} + \left\langle \mathcal{P}^{h\tau_1}_{r,e} \right\rangle_{U,2} = \frac{1}{V_e} \sum_{a,b} B^{ab}_{ij,kj} \left(I^{ab}_{ik} - G^{ab}_{ik} \right), \tag{62}$$

where summation on the spatial dimension indexes i, j, k is assumed whereas summation on nodes will be explicitly indicated throughout the text for the sake of clarity.

Pressure term $\left\langle \mathcal{P}^{h\tau_1}_{r,e} \right\rangle_P$ corresponding to the velocity subscales (42). It will be next found an expression similar to (62) but for the pressure term $\left\langle \mathcal{P}^{h\tau_1}_{r,e} \right\rangle_P$. Making use of (49) and (50) in (42), we get for the term in the second line of (42), which we denote $\left\langle \mathcal{P}^{h\tau_1}_{r,e} \right\rangle_{P,1}$,

$$\begin{aligned} \left\langle \mathcal{P}^{h\tau_1}_{r,e} \right\rangle_{P,1} &= \frac{1}{V_e} \left\langle \int_{\Omega_e} \left[\sum_a \partial_i N^a P^a \sum_b \partial_j N^b U^b_j U^b_i \right] d\Omega_e \right\rangle \\ &= \frac{1}{V_e} \left[\sum_{a,b} \left\langle P^a U^b_j U^b_i \right\rangle \int_{\Omega_e} \partial_i N^a \partial_j N^b d\Omega_e \right]. \end{aligned} \tag{63}$$

Using now (49), (50) and (55) in the third line of (42), we obtain

$$\begin{aligned} \left\langle \mathcal{P}^{h\tau_1}_{r,e} \right\rangle_{P,2} &= -\frac{1}{V_e} \left\langle \int_{\Omega_e} \left[\sum_{a,c} \mathcal{M}^{-1}_{cc} N^c \int_\Omega N^c \partial_i N^a P^a d\Omega \sum_b \partial_j N^b U^b_j U^b_i \right] d\Omega_e \right\rangle \\ &= -\frac{1}{V_e} \left\{ \sum_{a,b} \left\langle P^a U^b_j U^b_i \right\rangle \int_{\Omega_e} \left[\partial_j N^b \sum_c \mathcal{M}^{-1}_{cc} N^c \int_\Omega N^c \partial_i N^a d\Omega \right] d\Omega_e \right\}. \end{aligned} \tag{64}$$

Given the geometric factors (58)-(59) and defining the two point triple velocity-pressure correlation as

$$B^{ab}_{p,ij} = \left\langle P^a U^b_i U^b_j \right\rangle, \tag{65}$$

we can rewrite $\left\langle \mathcal{P}^{h\tau_1}_{r,e} \right\rangle_P$ as

$$\left\langle \mathcal{P}^{h\tau_1}_{r,e} \right\rangle_P = \left\langle \mathcal{P}^{h\tau_1}_{r,e} \right\rangle_{P,1} + \left\langle \mathcal{P}^{h\tau_1}_{r,e} \right\rangle_{P,2} = \frac{1}{V_e} \sum_{a,b} B^{ab}_{p,ij} \left(I^{ab}_{ij} - G^{ab}_{ij} \right), \tag{66}$$

with summation implied on indexes i, j.

Divergence term $\left\langle \mathcal{P}^{h\tau_2}_{r,e} \right\rangle$ corresponding to the pressure subscales (44). It can be readily checked that the expression analogous to (62) and (66) for the term $\left\langle \mathcal{P}^{h\tau_2}_{r,e} \right\rangle$ in (44) is given by

$$\left\langle \mathcal{P}^{h\tau_2}_{r,e} \right\rangle = \frac{1}{V_e} \sum_{a,b} B^{ab}_{ij} \left(I^{ab}_{ij} - G^{ab}_{ij} \right), \tag{67}$$

with B_{ij}^{ab} being the second-order velocity correlations (60).

Finite element expression for $\left\langle \mathcal{P}_{r,e}^{h\tau} \right\rangle$. Using the developments (62), (66) and (67) in equations (43) and (45) we obtain the finite element expression for the ensemble average of the rate of production of subgrid kinetic energy

$$\begin{aligned}\left\langle \mathcal{P}_{r,e}^{h\tau} \right\rangle &= \tau_{1,ae} \left\langle \mathcal{P}_{r,e}^{h\tau_1} \right\rangle + \tau_{2,ae} \left\langle \mathcal{P}_{r,e}^{h\tau_2} \right\rangle \\ &= \frac{1}{V_e} \sum_{a,b} \left[\tau_{1,ae} \left(B_{ij,kj}^{ab} + B_{p,ik}^{ab} \right) + \tau_{2,ae} B_{ik}^{ab} \right] \left(I_{ik}^{ab} - G_{ik}^{ab} \right). \end{aligned} \tag{68}$$

4 Relation between numerical subgrid kinetic energy transfer and physical dissipation in the inertial subrange

4.1 Two point fourth-order velocity correlations for $\left\langle \mathcal{P}_{r,e}^{h\tau_1} \right\rangle_U$

Given that I_{ij}^{ab} and G_{ij}^{ab} in (58)-(59) are pure geometric factors, in order to relate the expression (68) for $\left\langle \mathcal{P}_{r,e}^{h\tau} \right\rangle$ with the physical molecular dissipation, $\varepsilon_{\mathrm{mol}}$, we will have to relate the various second-order and fourth-order velocity correlations B_{ij}^{ab}, $B_{ij,kl}^{ab}$ and the two point triple velocity-pressure correlation $B_{p,ij}^{ab}$ to it.

To do so, use will be made in what follows of some results of statistical fluid mechanics and in particular of statistics concerning homogeneous isotropic turbulence. Although the various correlations B_{ij}^{ab}, $B_{ij,kl}^{ab}$ and $B_{p,ij}^{ab}$ do not involve the whole velocity and pressure fields at the nodes, but their OSS finite element approximation, we will consider that the results from statistical fluid mechanics can be still applied to them, similarly to what is assumed for the filtered velocity in a LES model. Note that in the case of $[\boldsymbol{u}_h, p_h]$ being the interpolant, see (48), no approximation would be needed. We then guess that the velocity and pressure from the OSS finite element solution will not differ substantially from the interpolant, at least in what concerns their statistical behavior. This is also implicitly assumed in practical implementations of the results in [13].

Let us start with the two point fourth moment velocity correlation $B_{ij,kl}^{ab}$, which by virtue of its definition (61) fulfills

$$B_{ij,kl}^{ab} = B_{ji,kl}^{ab} = B_{ji,lk}^{ab} = B_{ij,lk}^{ab}. \tag{69}$$

Use can be made of the *quasi-normal* approximation (*Millionshchikov zero-fourth-cumulant hypothesis*, see e.g., [41]) in order to relate the fourth-order velocity correlations with second-order velocity correlations. For the particular case of velocities being considered at just two points, the quasi-normal approximation for the exact velocity field establishes

$$\left\langle u_i^a u_j^a u_k^b u_l^b \right\rangle = \left\langle u_i^a u_j^a \right\rangle \left\langle u_k^b u_l^b \right\rangle + \left\langle u_i^a u_k^b \right\rangle \left\langle u_j^a u_l^b \right\rangle + \left\langle u_i^a u_l^b \right\rangle \left\langle u_j^a u_k^b \right\rangle. \tag{70}$$

Assuming that this relation holds true for the finite element velocity field, we can rewrite it using the notation (60)-(61) to obtain

$$B_{ij,kl}^{ab} = B_{ij}^{aa} B_{kl}^{bb} + B_{ik}^{ab} B_{jl}^{ab} + B_{il}^{ab} B_{jk}^{ab}. \tag{71}$$

In our case, the two-point fourth-order velocity correlation in (62) and (68) is contracted on the second and fourth indexes so that

$$B_{ij,kj}^{ab} = B_{ij}^{aa} B_{kj}^{bb} + B_{ik}^{ab} B_{jj}^{ab} + B_{ij}^{ab} B_{jk}^{ab}. \tag{72}$$

The second-order velocity correlations can be related to the second-order velocity structure function D_{ij}^{ab} defined by (see e.g., [41, 42])

$$D_{ij}^{ab} = \left\langle \left(U_i^b - U_i^a \right) \left(U_j^b - U_j^a \right) \right\rangle . \tag{73}$$

Developing (73) and under the assumption of homogeneous isotropic turbulence (which implies that $B_{ij}^{ab} = B_{ij}^{ba}$, $B_{ij}^{aa} = B_{ij}^{bb}$, see for example [41]) it is straightforward to see that

$$B_{ij}^{ab} = B_{ij}^{aa} - \frac{1}{2} D_{ij}^{ab} = \frac{1}{3} \left| \boldsymbol{U} \right|^2 \delta_{ij} - \frac{1}{2} D_{ij}^{ab}, \tag{74}$$

with $\boldsymbol{U}$ representing the ensemble average of the velocity either at node a or b, since both must be the same.

Substituting (74) into (72) yields

$$B_{ij,kj}^{ab} = \frac{5}{9} \left| \boldsymbol{U} \right|^4 \delta_{ik} - \frac{5}{6} \left| \boldsymbol{U} \right|^2 D_{ik}^{ab} - \frac{1}{6} \left| \boldsymbol{U} \right|^2 \delta_{ik} D_{jj}^{ab} + \frac{1}{4} \left(D_{jj}^{ab} D_{ik}^{ab} + D_{ij}^{ab} D_{jk}^{ab} \right). \tag{75}$$

The first term in (75) can be neglected in what follows given that it will vanish when finally inserted in (62). This is so because it can be factorized out of the summation on nodes in this expression. The summation can be carried inside the integrals in (58)-(59), which will then contain terms of the type $\partial_i \left(\sum_a N^a \right)$. Given that the shape functions form a partition of unity, $\sum_a N^a = 1$ and the derivative of this term is obviously zero (velocity boundary conditions need not to be considered at this point).

As previously mentioned, a computational mesh with its characteristic length h lying in the inertial subrange $[\, l_{DI}, l_{EI}]$ is considered in this paper. Combining the Kolmogorov first and second similarity hypothesis, an expression for the second order structure function D_{ij}^{ab} can be found solely in terms of $\varepsilon_{\mathrm{mol}}$ and the distance between nodes $\boldsymbol{x}^a$ and $\boldsymbol{x}^b$, $r^{ab} = \left\| \boldsymbol{x}^a - \boldsymbol{x}^b \right\|$, for $r^{ab} \in [\, l_{DI}, l_{EI}]$. The expression is given by (see e.g., [41, 42])

$$D_{ij}^{ab} = 2C \left(\varepsilon_{\mathrm{mol}} r^{ab} \right)^{2/3} \mathcal{D}_{ij}^{ab}, \quad \mathcal{D}_{ij}^{ab} := \frac{1}{6} \left(4\delta_{ij} - \frac{r_i^{ab} r_j^{ab}}{(r^{ab})^2} \right), \tag{76}$$

where C represents a universal constant with approximate value $C \approx 2$. Substituting (76) in (75) gives

$$\begin{aligned} B_{ij,kj}^{ab} = -\frac{11}{18} \left| \boldsymbol{U} \right|^2 C \left(\varepsilon_{\mathrm{mol}} r^{ab} \right)^{2/3} \delta_{ik} + \Bigg[-\frac{5}{3} \left| \boldsymbol{U} \right|^2 C \left(\varepsilon_{\mathrm{mol}} r^{ab} \right)^{2/3} \\ + \frac{11}{6} C^2 \left(\varepsilon_{\mathrm{mol}} r^{ab} \right)^{4/3} \Bigg] \mathcal{D}_{ik}^{ab} + C^2 \left(\varepsilon_{\mathrm{mol}} r^{ab} \right)^{4/3} \mathcal{D}_{ij}^{ab} \mathcal{D}_{jk}^{ab}. \end{aligned} \tag{77}$$

We can now make use again of Kolmogorov's second similarity hypothesis, which as explained in section 3.1.1 states that for an eddy of size $\ell \in [l_{DI}, l_{EI}]$ (i.e. lying in the inertial subrange) all velocity scales are proportional to $\left(\varepsilon_{\mathrm{mol}} \ell \right)^{1/3}$. Since $|\boldsymbol{U}|$ is a velocity, it follows that

$$|\boldsymbol{U}| \sim \left(\varepsilon_{\mathrm{mol}} \ell \right)^{1/3} \tag{78}$$

and substituting in (77)

$$\begin{aligned} B_{ij,kj}^{ab} = C \varepsilon_{\mathrm{mol}}^{4/3} \Bigg\{ -\frac{11}{18} \ell^{2/3} \left(r^{ab} \right)^{2/3} \delta_{ik} + \Bigg[-\frac{5}{3} \ell^{2/3} \left(r^{ab} \right)^{2/3} \\ + \frac{11}{6} C \left(r^{ab} \right)^{4/3} \Bigg] \mathcal{D}_{ik}^{ab} + C \left(r^{ab} \right)^{4/3} \mathcal{D}_{ij}^{ab} \mathcal{D}_{jk}^{ab} \Bigg\} =: \varepsilon_{\mathrm{mol}}^{4/3} \mathcal{K}_{ik}^{ab}, \end{aligned} \tag{79}$$

where $\mathcal{K}_{ik}^{ab}$ has been defined in the last line of (79).

In view of (79), equation (62) for $\left\langle \mathcal{P}_{r,e}^{h\tau_1} \right\rangle_U$ can be rewritten as

$$\left\langle \mathcal{P}_{r,e}^{h\tau_1} \right\rangle_U = \frac{1}{V_e} \varepsilon_{\text{mol}}^{4/3} \sum_{a,b} \mathcal{K}_{ik}^{ab} \left(I_{ik}^{ab} - G_{ik}^{ab} \right). \tag{80}$$

4.2 Two point triple-order velocity-pressure correlations for $\left\langle \mathcal{P}_{r,e}^{h\tau_1} \right\rangle_P$

It is our aim now to find an expression analogous to (80) but relating the two point triple-order velocity-pressure correlation $B_{p,ij}^{ab}$ with the rate of physical dissipation ε_{mol}. To do so we will closely follow [41] although with some particularities. We will abuse of notation and use $B_{p,ij}^{ab}$ to denote the triple-order velocity-pressure correlations of either the exact velocity field or the finite element approximated one. Whether equations are valid for one or the other, or for both of them, can be easily determined by the context. Likewise, we will identify $r \equiv r^{ab}$, being clear that this is the distance between nodes $\boldsymbol{x}^a$ and $\boldsymbol{x}^b$.

The tensor of second rank $B_{p,kl}^{ab}$ for the isotropic case can be written as

$$B_{p,kl}^{ab} = P_1(r)\, r_k r_l + P_2(r)\, \delta_{kl}, \tag{81}$$

where

$$P_1(r) = \frac{1}{r^2} \left[B_{p,LL}^{ab} - B_{p,NN}^{ab} \right], \quad P_2(r) = B_{p,NN}^{ab}, \tag{82}$$

with the subscript L standing for *longitudinal* and designating the direction of the vector $\boldsymbol{r}^{ab}$ and N standing for *normal* and designating any perpendicular direction to it.

Consider the Poisson equation for the pressure at node a

$$\Delta p = -\partial_{r_i} \partial_{r_j} \left(u_i^a u_j^a \right) \tag{83}$$

where Δ is the Laplacian operator that for functions only depending on r becomes

$$\Delta = \frac{d^2}{dr^2} + \frac{2}{r} \frac{d}{dr}. \tag{84}$$

Multiplying both sides of (83) by $u_k^b u_l^b$ and performing an ensemble average of the results yields

$$\Delta B_{p,kl}^{ab} = -\partial_{r_i} \partial_{r_j} \left(B_{ij,kl}^{ab} \right). \tag{85}$$

In the case of homogeneous isotropic turbulence, the tensor in the r.h.s of (85) is an isotropic symmetric tensor of second rank that can be expressed as

$$\partial_{r_i} \partial_{r_j} \left(B_{ij,kl}^{ab} \right) = Q_1(r)\, r_k r_l + Q_2(r)\, \delta_{kl}. \tag{86}$$

Inserting (81) and (86) in (85) and equating the coefficients of $r_k r_l$ and δ_{kl} on both sides yields two differential equations for the unknowns P_1 and P_2:

$$\frac{d^2 P_1}{dr^2} + \frac{6}{r} \frac{dP_1}{dr} = -Q_1. \tag{87}$$

$$\frac{d^2 P_2}{dr^2} + \frac{2}{r} \frac{dP_2}{dr} + 2P_1 = -Q_2. \tag{88}$$

These equations can be uncoupled defining a new function P_3 such that

$$P_3(r) = r^2 P_1(r) + 3P_2(r) = B^{ab}_{p,LL} + 2B^{ab}_{p,NN}. \tag{89}$$

Multiplying (87) by r^2 and adding the result to (88) multiplied by 3 gives the following equation for P_3:

$$\frac{d^2 P_3}{dr^2} + \frac{2}{r}\frac{dP_3}{dr} = -Q_3, \tag{90}$$

where

$$Q_3(r) = r^2 Q_1(r) + 3Q_2(r). \tag{91}$$

In order to find the two point triple-order velocity-pressure correlation $B^{ab}_{p,kl}$ in (81) we need the values of P_1 and P_2, which can be obtained from the solutions of the equations (87) and (90) together with (89). However, to solve these equations we first need a value for their inhomogeneous terms Q_1 and Q_3. To do so, the use of the quasi-normal approximation and of Kolmogorov's similarity hypotheses will prove very useful again. We remind that our interest is in finding the results for r in the inertial subrange $[l_{DI}, l_{EI}]$.

Making use of the quasi-normal approximation (71) in (86) and taking into account that due to the incompressibility constraint $\partial_{r_i} B^{ab}_{ij} = \partial_{r_j} B^{ab}_{ij} = 0$ (see [41]), it follows that

$$Q_1(r)\, r_k r_l + Q_1(r)\, \delta_{kl} = \partial_{r_i}\partial_{r_j}\left(B^{ab}_{ij,kl}\right) = 2\partial_{r_j} B^{ab}_{ik}\partial_{r_i} B^{ab}_{jl} \tag{92}$$

and given that the second-order velocity correlation tensor B^{ab}_{ij} for homogeneous isotropic turbulence can be expressed as [41]

$$B^{ab}_{ij} = -\partial_r B^{ab}_{LL}(r)\frac{r_i r_j}{r} + \left[B^{ab}_{LL}(r) + \frac{r}{2}\partial_r B^{ab}_{LL}\right], \tag{93}$$

we can obtain the following expressions for Q_1, Q_2 and Q_3 solely in terms of the longitudinal second-order velocity correlation B^{ab}_{LL}:

$$Q_1(r) = \frac{6}{r^2}\left[\frac{d}{dr}B^{ab}_{LL}(r)\right]^2 + \frac{1}{r}\frac{d}{dr}B^{ab}_{LL}(r)\frac{d^2}{dr^2}B^{ab}_{LL}(r), \tag{94}$$

$$Q_2(r) = -3\left[\frac{d}{dr}B^{ab}_{LL}(r)\right]^2 - r\frac{d}{dr}B^{ab}_{LL}(r)\frac{d^2}{dr^2}B^{ab}_{LL}(r), \tag{95}$$

$$Q_3(r) = -\frac{1}{r^2}\frac{d}{dr}\left\{r^3\left[\frac{d}{dr}B^{ab}_{LL}(r)\right]^2\right\}. \tag{96}$$

Use has been made of (91) to obtain the expression for Q_3.

Up to know we have followed [41], which should be consulted for details. We can next use (74) to relate B^{ab}_{LL} with the longitudinal velocity structure function D^{ab}_{LL} and the rate of dissipation $\varepsilon_{\mathrm{mol}}$:

$$B^{ab}_{LL} = B^{aa}_{LL} - \frac{1}{2}D^{ab}_{LL} = B^{aa}_{LL} - \frac{C}{2}\left(\varepsilon_{\mathrm{mol}} r\right)^{2/3}. \tag{97}$$

Substituting (97) in (94) and (96) results in

$$Q_1(r) = \frac{17}{27}C^2\varepsilon_{\mathrm{mol}}^{4/3} r^{-8/3}, \tag{98}$$

$$Q_3(r) = -\frac{7}{27}C^2\varepsilon_{\mathrm{mol}}^{4/3} r^{-2/3}. \tag{99}$$

The solutions to equations (87) and (90) with the inhomogeneous terms given by (98) and (99) and appropriate boundary conditions can be found using the Green's function approach. This yields (see Appendix)

$$P_1(r) = -\frac{17}{27} C^2 \varepsilon_{\text{mol}}^{4/3} F_1^{ab}(r), \tag{100}$$

$$P_3(r) = \frac{1}{27} C^2 \varepsilon_{\text{mol}}^{4/3} F_3^{ab}(r) \tag{101}$$

where $F_1^{ab}(r)$ an $F_3^{ab}(r)$ are functions only depending on the distance r.

We can next obtain $P_2(r) = B_{p,NN}^{ab}(r)$ substituting (100) and (101) into (89):

$$\begin{aligned} P_2(r) := \frac{1}{81} C^2 \varepsilon_{\text{mol}}^{4/3} \Big\{ & 17 F_{01} r^{-3} + 7 F_{03} r^{-1} + 7 F_{13} \\ & + \left[17 F_{11} + 7 F_{23} r^{4/3} \right] + 17 F_{21} r^2 \Big\} =: \frac{1}{81} C^2 \varepsilon_{\text{mol}}^{4/3} F_{NN}^{ab}(r), \end{aligned} \tag{102}$$

where the values of the various terms F_{ij} in (102) are given in the Appendix (equations (A.10)-(A.12), (A.22)-(A.24)) and F_{NN}^{ab} has been defined in the last step.

Inserting (100) and (102) in (81) we find the expression for the two-point triple order velocity-pressure correlation $B_{p,ij}^{ab}$ we were looking for:

$$\begin{aligned} B_{p,ij}^{ab} &= P_1(r) r_i r_j + P_2(r) \delta_{ij} \\ &= \frac{1}{27} C^2 \varepsilon_{\text{mol}}^{4/3} \left[17 F_1^{ab}(r) r_i r_j + \frac{1}{3} F_{NN}^{ab}(r) \delta_{ij} \right] \\ &=: \varepsilon_{\text{mol}}^{4/3} \mathcal{F}_{ij}^{ab}(r), \end{aligned} \tag{103}$$

$\mathcal{F}_{ij}^{ab}(r)$ being defined in the last line.

Finally, we can find an expression for the numerical kinetic energy transfer term $\left\langle \mathcal{P}_{r,e}^{h\tau_1} \right\rangle_P$ in equation (66). Substituting (103) in (66) yields

$$\left\langle \mathcal{P}_{r,e}^{h\tau_1} \right\rangle_P = \frac{1}{V_e} \varepsilon_{\text{mol}}^{4/3} \sum_{a,b} \mathcal{F}_{ij}^{ab} \left(I_{ij}^{ab} - G_{ij}^{ab} \right). \tag{104}$$

4.3 Two point second-order velocity correlations for $\left\langle \mathcal{P}_{r,e}^{h\tau_2} \right\rangle$

The last term that has to be dealt with is $\left\langle \mathcal{P}_{r,e}^{h\tau_2} \right\rangle$ in (67) arising from the pressure subscales stabilization. As seen, (67) only involves the second-order velocity correlation tensor B_{ij}^{ab}. From (74) and (76) it can readily be checked that the expression analogous to (80) and (104) for the term $\left\langle \mathcal{P}_{r,e}^{h\tau_2} \right\rangle$ in (67) is given by

$$\begin{aligned} \left\langle \mathcal{P}_{r,e}^{h\tau_2} \right\rangle_P &= \frac{2C}{V_e} \varepsilon_{\text{mol}}^{2/3} \sum_{a,b} r^{2/3} \mathcal{D}_{ij}^{ab} \left(I_{ij}^{ab} - G_{ij}^{ab} \right) \\ &=: \frac{1}{V_e} \varepsilon_{\text{mol}}^{2/3} \sum_{a,b} \widetilde{\mathcal{D}}_{ij}^{ab} \left(I_{ij}^{ab} - G_{ij}^{ab} \right), \end{aligned} \tag{105}$$

with $\widetilde{\mathcal{D}}_{ij}^{ab} := 2C r^{2/3} \mathcal{D}_{ij}^{ab}$.

4.4 Relation between $\left\langle \mathcal{P}_{r,e}^{h\tau} \right\rangle$ and the physical rate of dissipation $\varepsilon_{\rm mol}$

From equations (80), (104) and (105) substituted in (68) we get

$$\left\langle \mathcal{P}_{r,e}^{h\tau} \right\rangle = \frac{1}{V_e} \sum_{a,b} \left[\tau_{1,ae} \varepsilon_{\rm mol}^{4/3} \left(\mathcal{K}_{ik}^{ab} + \mathcal{F}_{ik}^{ab} \right) + \tau_{2,ae} \varepsilon_{\rm mol}^{2/3} \widetilde{\mathcal{D}}_{ik}^{ab} \right] \left(I_{ik}^{ab} - G_{ik}^{ab} \right) \tag{106}$$

and finally inserting expressions (37)-(38) for the stabilization parameters in (106) we obtain the final expression we were looking for

$$\left\langle \mathcal{P}_{r,e}^{h\tau} \right\rangle = \varepsilon_{\rm mol} \left\{ \frac{h}{V_e} \sum_{a,b} \left[\ell^{-1/3} \left(\mathcal{K}_{ik}^{ab} + \mathcal{F}_{ik}^{ab} \right) + \ell^{1/3} \widetilde{\mathcal{D}}_{ik}^{ab} \right] \left(I_{ik}^{ab} - G_{ik}^{ab} \right) \right\}, \tag{107}$$

which states that the average value of $\mathcal{P}_r^{h\tau}$ on a mesh element is directly related to the molecular physical dissipation by means of a factor that only depends on the mesh geometry and the interpolation spaces used to approximate the continuous ones. Note that, for $\ell \geq Ch$, with $C > 1$ dimensionless, the factor that multiplies $\varepsilon_{\rm mol}$ is purely geometrical (and of course dimensionless).

5 Discussion and remarks

5.1 General comments

In section 2.3.3 we wondered about the possibility that some terms in $\mathcal{P}_r^{h\tau}$ integrated over the whole computational domain equated the overall physical dissipation in the energy balance equation. It was argued that this should not necessarily be the case for all the stabilization terms in $\mathcal{P}_r^{h\tau}$, given that they arise from purely numerical considerations rather than physical ones. However, we have found in (107) that when using the OSS stabilized finite element method all terms in the ensemble average of $\mathcal{P}_r^{h\tau}$ are proportional to the dissipation $\varepsilon_{\rm mol}$. This can be viewed as a confirmation of the right choice for the stabilization parameters τ_1 and τ_2 in the OSS formulation.

As observed from (107) the proportionality factor between $\left\langle \mathcal{P}_{r,e}^{h\tau} \right\rangle$ and $\varepsilon_{\rm mol}$ is a rather complicated function depending on the element and mesh geometry, as well on the chosen finite element interpolation spaces. Although one could be tempted to think that its optimum value should equal unity in order to have the desired physical behavior, we have no basis to assess this point given that, as stated, the terms in (107) have to account not only for appropriate physical behavior, but also for circumventing purely numerical difficulties (e.g., to allow the use of equal interpolation spaces for the velocity and the pressure).

In any case, what seems to follow from the above analysis is that it makes somehow redundant and unnecessary the use of LES models. Effectively, should we have done the above analysis for the energy balance equation (34), a result of the type $\overline{\mathcal{P}}_r^{h\tau} = \alpha \varepsilon_{\rm mol}$ (with α being a proportionality function analogous to the one in (107)) would have been obtained. On the other hand, the term arising from the LES model would also behave as $\overline{\mathcal{P}}_r^{h} = \beta \varepsilon_{\rm mol}$ so that its effects, if any, could be included in the $\overline{\mathcal{P}}_r^{h\tau}$ term with appropriate redefinition of the proportionality factor. Hence, if a good enough discretization of the Navier-Stokes equations is performed, the somehow artificial fact of filtering and modeling at the continuous level should be unnecessary. In other words, the problem of simulating turbulence is probably a purely numerical problem of correctly discretizing the Navier-Stokes equations rather than a problem of LES physical modeling.

5.2 Other numerical approaches

As it has been mentioned, the purely numerical strategy to simulate turbulent flows is not new, and can be traced back (at least) to the MILES approach. Sometimes, these type of models are referred to as *implicit LES* models. Some examples of them can be found in [43]. In these type of methods, the subgrid-scale stress tensor is modeled depending on the numerical procedure. For example, in [14] the model proposed is based on the parallel solution of the truncated Navier-Stokes equations on a mesh twice smaller in each Cartesian direction than the one used to compute the resolved quantities. In this method, the subgrid velocity is computed at each time step, without accounting for its time evolution, and its expression is used to evaluate the subgrid-scale stress tensor. One of the conclusions that can be drawn from the numerical results presented is that the method does not have enough dissipation. In an attempt to overcome this misbehavior, the parameters on which the formulation depends could be adjusted so as to follow the correct dissipation structure, as proposed in [25], where the spectra of the numerical solution and the physical one are forced to match for isotropic turbulence.

A fundamental difference between the approaches described and the one we have analyzed here is that *we do not model neither the subgrid scale stress tensor nor its effect*. Rather, we simply add terms based on the effect of the subscales onto the finite element component of the solution. As we have shown, the overall effect is a dissipation that mimics the physical one. In this sense, our approach has to be considered *residual based*, as the one proposed in [1] and also in [26, 44]. In this case, the terms added to the Galerkin formulation of the problem depend on the residual of the finite element solution, which is thus considered the resolved scale. In contrast to our approach with *orthogonal* subscales, in the references mentioned the subscales are considered directly proportional to the finite element residual. This implies that the orthogonal projection is dropped in (23) and (24). This fact has an important consequence in the energy balance equation (28), since both the coefficients of the time variation of kinetic energy and the power of the external forces will change. The OSS method simplifies the analysis, but nevertheless the dissipative terms which we have shown are proportional to the molecular dissipation *are also present in the method of [1]*.

5.3 Numerical evidence

The starting assumption of our analysis is that the finite element mesh is able to capture velocity fields that lay in the inertial range and for which the results of statistical fluid mechanics can be applied. This condition should not be considered particularly stringent, as it is in fact analogous to what is assumed for the filtered velocity in classical LES models for which the filter width is proportional to (if not directly equal) the mesh size. Moreover, there is already some sound numerical evidence that this is in fact possible and that residual based numerical formulations can model turbulence flows.

A relevant numerical study of a residual based formulation modeling turbulent flows is [1]. The formulation is tested for isotropic forced turbulence and turbulent channel flows and the results are extremely good, in the sense that they clearly display the numerical convergence towards results from direct numerical simulation (DNS). Both mesh refinement and polynomial order increase (using NURBS) are tested. In the case of isotropic turbulence, for coarse discretizations the numerical spectra match the DNS results only for small wave numbers, whereas the matching improves as the discretization is also improved. The important point, however, is that even for coarse discretizations *there is part of the inertial range which is captured* and, of course, with the correct slope, a characteristic feature of turbulent flows. For channel flows it is also shown that the boundary layers that are created have the regions corresponding to turbulence.

It is not the purpose of this paper to present a detailed numerical study of the behavior of the OSS formulation to model turbulent flows. However, we shall present here a simple example to compare the numerical response of this formulation alone and in conjunction with the classical Smagorinsky model.

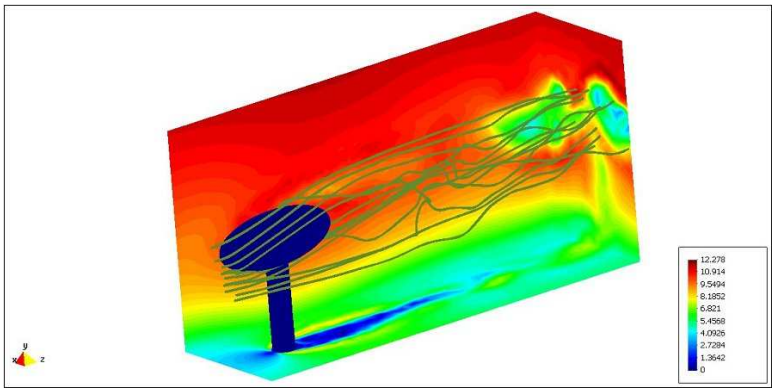

Figure 1: Flow over a circular plate. Streamlines and contours of the velocity norm. Inlet velocity = 10 m/s.

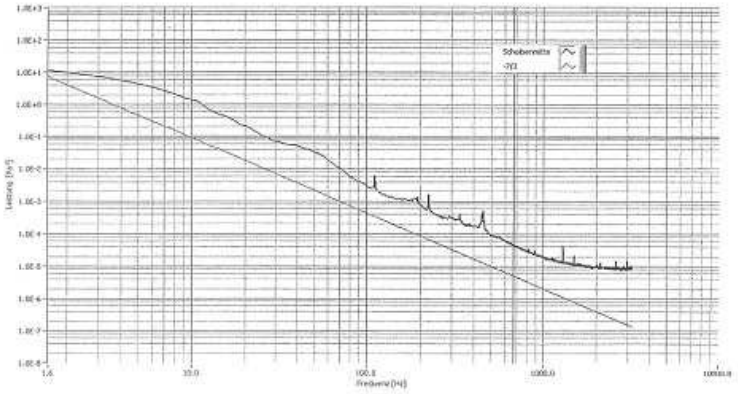

Figure 2: Experimental pressure spectrum (theoretical slope = $-7/3$). Courtesy of GBF Aachen, Dipl. Ing. Ralf Haase.

For that purpose, we consider the example of the flow over a circular plate. The general view of the computational domain, together with some streamlines and the contours of the Euclidean norm of the velocity field, are shown in Fig. 1. The flow comes from the left side of the computational domain, a box of $9 \times 2.5 \times 1.8$ m^3 in which the inclined circular plate with its support is placed, with a velocity of 10 m/s. The diameter of the plate is 0.5 m. The domain has been discretized with a rather coarse mesh of 1.34 million linear elements (more details about this numerical example can be found in [21]).

Our interest here is to reproduce the *pressure spectrum* at the center of the plate, for which experimental results are available [21]. The inertial range of the pressure spectrum should be proportional to the power $-7/3$ of the wave number and, assuming Taylor's hypothesis, the time spectrum should also be proportional to the power $-7/3$ of the frequency. This is the predicted power law behavior for the pressure spectrum of isotropic turbulence (see e.g. [39]). Experimental results, which confirm this fact, are shown in Fig. 2.

The important point is how is the pressure spectrum reproduced by the OSS formulation alone and with the Smagorinsky model. From Fig. 3 (top) it is seen that in both cases the $-7/3$ slope is reproduced, confirming that the approximated fields belong to the inertial range. The qualitative difference between turning off or on the Smagorinsky model can also be observed from Fig. 3 (bottom). It is seen that, in spite of the fact that both possibilities yield the correct slope of the pressure spectrum, the OSS

formulation alone has a richer dynamic response of the pressure, thus confirming that turning on the Smagorinsky model introduces a dissipation that adds up to one that is already physically correct.

6 Conclusions

For a fine enough computational mesh, it has been proved that the contribution to the energy balance equation of the stabilization terms of the Orthogonal Subgrid Scale stabilized finite element method is already proportional to the physical dissipation rate for an appropriate choice of the stabilization parameters. This has been done with the sole use of the quasi-normal approximation for two point fourth-order velocity correlations and using Kolmogorov's first and second similarity hypotheses. It has been also assumed that several statistical fluid mechanics results, which are valid for the exact velocity field, hold true for the approximated finite element velocity field.

Taking into account that the stabilization terms in the OSS method arise from pure numerical necessities it is a noteworthy fact that they have the correct physical behavior in the inertial subrange of a turbulent flow. This somehow supports the idea that no extra physical LES modeling should be added to the equations if an appropriate stabilization method is used. That is to say, the simulation of turbulence should probably rely on optimum numerical modeling rather than in physical one.

Appendix. Green's function approach to obtain $P_1(r)$ and $P_3(r)$

We will first address the problem of finding the solution $P_1(r)$ of the inhomogeneous equation (87) in text using the Green's function approach. The solutions to the homogeneous counterpart of (87) are 1 and r^{-5} so that the problem Green's function will be of the type

$$G_1(r,r_0) = \begin{cases} A + Br^{-5} \equiv G_1^{<}(r,r_0) & l_{DI} < r < r_0 \\ \\ C + Dr^{-5} \equiv G_1^{>}(r,r_0) & r_0 < r < l_{EI}\,. \end{cases} \tag{A.1}$$

To determine the values of A, B, C and D we impose the boundary conditions at the inertial range threshold values $[l_{DI}, l_{EI}]$

$$G_1(l_{DI},r_0) = K_{D1}, \tag{A.2}$$
$$G_1(l_{EI},r_0) = K_{E1}, \tag{A.3}$$

with K_{D1}, K_{E1} constants. We also impose the continuity conditions

$$G_1^{>}\left(r_0^{+},r_0\right) - G_1^{<}\left(r_0^{-},r_0\right) = 0 \tag{A.4}$$
$$\partial_r G_1^{>}\left(r_0^{+},r_0\right) - \partial_r G_1^{<}\left(r_0^{-},r_0\right) = -1 \tag{A.5}$$

with $G_1^{\gtrless}\left(r_0^{\pm},r_0\right) \equiv \lim_{\substack{r\to r_0 \\ r\gtrless r_0}} G_1^{\gtrless}(r,r_0)$. Defining the constants

$$L_{\Delta E} := \frac{l_{EI}^5}{l_{EI}^5 - l_{DI}^5}, \quad L_{\Delta D} := \frac{l_{DI}^5}{l_{EI}^5 - l_{DI}^5}, \quad L_{ED} := \frac{l_{EI}^5 l_{DI}^5}{l_{EI}^5 - l_{DI}^5}, \tag{A.6}$$

as well as

$$A_{01} := L_{\Delta E}K_{E1} - L_{\Delta D}K_{D1}, \quad A_{11} := -L_{ED}\left(K_{E1} - K_{D1}\right), \quad A_{21} := -\frac{L_{ED}}{l_{EI}^5 l_{DI}^5}, \tag{A.7}$$

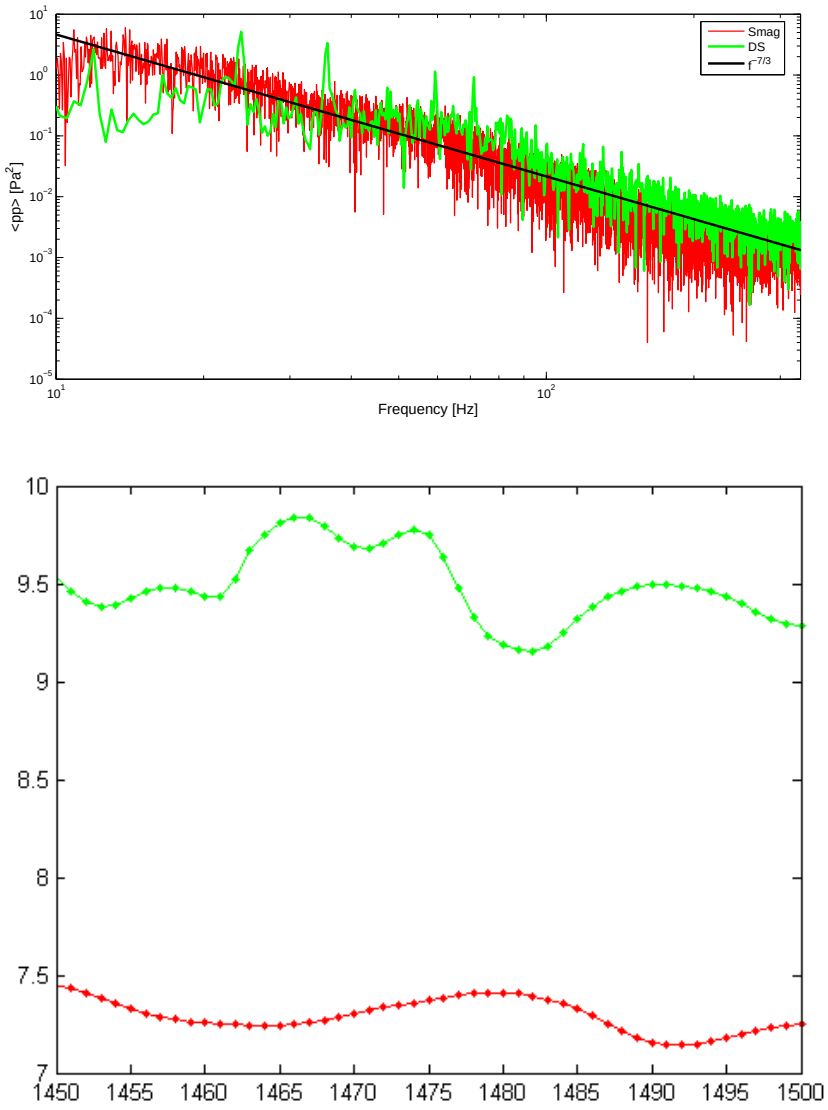

Figure 3: Comparison of the OSS formulation without (green) and with the Smagorinsky model (red). Top: numerical pressure spectrum (theoretical slope = $-7/3$), Bottom: detail of the pressure evolution (at the center of the plate).

it can readily be checked that the following expression is obtained for the Green function in (A.1)

$$G_1(r,r_0)=\begin{cases}\left(A_{01}+A_{11}r^{-5}\right)+\frac{1}{5}\left(L_{\Delta E}-L_{ED}r^{-5}\right)r_0 \\ +\frac{1}{5}\left(A_{21}+L_{\Delta D}r^{-5}\right)r_0^6 & l_{DI}<r<r_0 \\ & \\ \left(A_{01}+A_{11}r^{-5}\right)+\frac{1}{5}\left(L_{\Delta D}-L_{ED}r^{-5}\right)r_0 \\ +\frac{1}{5}\left(A_{21}+L_{\Delta E}r^{-5}\right)r_0^6 & r_0<r<l_{EI}\,.\end{cases} \tag{A.8}$$

Using (A.8) and the inhomogeneous term $Q_1(r)$ from equation (98) in text, $P_1(r)$ can be found as

$$\begin{aligned}P_1(r)&=-\int_{l_{DI}}^{r}G_1^{>}(r,r_0)\,Q_1(r_0)\,dr_0-\int_{r}^{l_{EI}}G_1^{<}(r,r_0)\,Q_1(r_0)\,dr_0\\&=-\frac{17}{27}C^2\varepsilon_{\text{mol}}^{4/3}\left[F_{01}\frac{1}{r^5}+F_{11}\frac{1}{r^{2/3}}+F_{21}\right]=:-\frac{17}{27}C^2\varepsilon_{\text{mol}}^{4/3}F_1^{ab}(r)\,,\end{aligned} \tag{A.9}$$

where

$$\begin{aligned}F_{01}&:=-\frac{3}{5}\left(l_{EI}^{-5/3}-l_{DI}^{-5/3}\right)A_{11}+\frac{3}{10}\left(l_{EI}^{-2/3}-l_{DI}^{-2/3}\right)L_{ED}\\&\quad+\frac{3}{65}\left(L_{\Delta D}l_{EI}^{13/3}-L_{\Delta E}l_{DI}^{13/3}\right),\end{aligned} \tag{A.10}$$

$$F_{11}:=\frac{33}{130}\left(L_{\Delta E}-L_{\Delta D}\right), \tag{A.11}$$

$$\begin{aligned}F_{21}&:=-\frac{3}{5}\left(l_{EI}^{-5/3}-l_{DI}^{-5/3}\right)A_{01}+\frac{3}{65}\left(l_{EI}^{13/3}-l_{DI}^{13/3}\right)A_{21}\\&\quad+\frac{3}{10}\left(L_{\Delta D}l_{DI}^{-2/3}-L_{\Delta E}l_{EI}^{-2/3}\right),\end{aligned} \tag{A.12}$$

and we have defined $F_1^{ab}(r)$ in the last line of (A.9).

We can now proceed analogously to find the solution $P_3(r)$ to equation (90) in the text. The solutions for the homogeneous counterpart of this equation are 1 and r^{-1} so that the Green function will behave as

$$G_3(r,r_0)=\begin{cases}A+Br^{-1}\equiv G_3^{<}(r,r_0) & l_{DI}<r<r_0\\ & \\ C+Dr^{-1}\equiv G_3^{>}(r,r_0) & r_0<r<l_{EI}\,.\end{cases} \tag{A.13}$$

To find A,B,C and D in (A.13) we impose the boundary conditions

$$G_3(l_{DI},r_0)=K_{D3}, \tag{A.14}$$

$$G_3(l_{EI},r_0)=K_{E3}, \tag{A.15}$$

as well as the continuity conditions

$$G_3^{>}\left(r_0^{+},r_0\right)-G_3^{<}\left(r_0^{-},r_0\right)=0 \tag{A.16}$$

$$\partial_r G_3^{>}\left(r_0^{+},r_0\right)-\partial_r G_3^{<}\left(r_0^{-},r_0\right)=-1. \tag{A.17}$$

Defining the new constants

$$\ell_{\Delta E}:=\frac{l_{EI}}{l_{EI}-l_{DI}},\quad \ell_{\Delta D}:=\frac{l_{DI}}{l_{EI}-l_{DI}},\quad \ell_{ED}:=\frac{l_{EI}l_{DI}}{l_{EI}-l_{DI}}, \tag{A.18}$$

and

$$A_{03} := \ell_{\Delta E} K_{E3} - \ell_{\Delta D} K_{D3}, \quad A_{13} := -\ell_{ED} \left(K_{E3} - K_{D3} \right), \quad A_{23} := -\frac{\ell_{ED}}{l_{EI} l_{DI}}, \tag{A.19}$$

the Green function (A.13) can be written as

$$G_3 \left(r, r_0 \right) = \begin{cases} \left(A_{03} + A_{13} r^{-1} \right) + \left(\ell_{\Delta E} - \ell_{ED} r^{-1} \right) r_0 \\ + \left(A_{23} + \ell_{\Delta D} r^{-1} \right) r_0^2 & l_{DI} < r < r_0 \\ \\ \left(A_{03} + A_{13} r^{-1} \right) + \left(\ell_{\Delta D} - \ell_{ED} r^{-1} \right) r_0 \\ + \left(A_{23} + \ell_{\Delta E} r^{-1} \right) r_0^2 & r_0 < r < l_{EI} \, . \end{cases} \tag{A.20}$$

We can now find $P_3 \left(r \right)$ using (A.20) and the inhomogeneous term $Q_3 \left(r \right)$ from equation (99) in text

$$\begin{aligned} P_3(r) &= \int_{l_{DI}}^{r} G_3^{>} \left(r, r_0 \right) Q_3 \left(r_0 \right) dr_0 + \int_{r}^{l_{EI}} G_3^{<} \left(r, r_0 \right) Q_3 \left(r_0 \right) dr_0 \\ &= \frac{7}{27} C^2 \varepsilon_{\text{mol}}^{4/3} \left[F_{03} \frac{1}{r} + F_{13} + F_{23} r^{4/3} \right] =: \frac{1}{27} C^2 \varepsilon_{\text{mol}}^{4/3} F_3^{ab} \left(r \right), \end{aligned} \tag{A.21}$$

where

$$\begin{aligned} F_{03} &:= 3 \left(l_{EI}^{1/3} - l_{DI}^{1/3} \right) A_{13} - \frac{3}{4} \left(l_{EI}^{4/3} - l_{DI}^{4/3} \right) \ell_{ED} \\ &\quad + \frac{3}{7} \left(\ell_{\Delta D} l_{EI}^{7/3} - \ell_{\Delta E} l_{DI}^{7/3} \right), \end{aligned} \tag{A.22}$$

$$\begin{aligned} F_{13} &:= 3 \left(l_{EI}^{1/3} - l_{DI}^{1/3} \right) A_{03} + \frac{3}{7} \left(l_{EI}^{7/3} - l_{DI}^{7/3} \right) A_{23} \\ &\quad - \frac{3}{4} \left(\ell_{\Delta D} l_{DI}^{4/3} - \ell_{\Delta E} l_{EI}^{4/3} \right), \end{aligned} \tag{A.23}$$

$$F_{21} := -\frac{9}{28} \left(\ell_{\Delta E} - \ell_{\Delta D} \right), \tag{A.24}$$

and $F_3^{ab} \left(r \right)$ has been defined in the last line of (A.21).

References

[1] Y. Bazilevs, V. Calo, J. Cottrell, T. Hughes, A. Reali, and G. Scovazzi. Variational multiscale residual-based turbulence modeling for large eddy simulation of incompressible flows. *Comput. Methods Appl. Mech. Engrg.*, 197:173–201, 2007.

[2] L. Berselli, T. Iliescu, and W. Layton. *Mathematics of Large Eddy Simulation of Turbulent Flows*. Springer-Verlag, 2006.

[3] J. Boris, F. Grinstein, E. Oran, and R. Kolbe. New insights into large eddy simulation. *Fluid Dyn. Res.*, 10:199–228, 1992.

[4] V. Calo. *Residual based multiscale turbulence modeling: finite volume simulations of bypass transition*. PhD thesis, Department of Civil and Environmental Engineering, Stanford University, 2004.

[5] F. Chow and P. Moin. A further study of numerical errors in large-eddy simulations. *J. Comput. Phys.*, 184:366–380, 2003.

[6] R. Codina. A nodal-based implementation of a stabilized finite element method for incompressible flow problems. *Int. J. Numer. Meth. Fluids*, 33:737–766, 2000.

[7] R. Codina. On stabilized finite element methods for linear systems of convection-diffusion-reaction equations. *Comput. Methods Appl. Mech. Engrg.*, 188:61–82, 2000.

[8] R. Codina. Stabilization of incompressibility and convection through orthogonal sub-scales in finite element methods. *Comput. Methods Appl. Mech. Engrg.*, 190:1579–1599, 2000.

[9] R. Codina. A stabilized finite element method for generalized stationary incompressible flows. *Comput. Methods Appl. Mech. Engrg.*, 190:2681–2706, 2001.

[10] R. Codina. Stabilized finite element approximation of transient incompressible flows using orthogonal subscales. *Comput. Methods Appl. Mech. Engrg.*, 191:4295–4321, 2002.

[11] R. Codina. Analysis of a stabilized finite element approximation of the Oseen equations using orthogonal subscales. *Appl. Numer. Math.*, 58:264–28, 2008.

[12] R. Codina, J. Principe, O. Guasch, and S. Badia. Time dependent subscales in the stabilized finite element approximation of incompressible flow problems. *Comput. Methods Appl. Mech. Engrg.*, 196:2413–2430, 2007.

[13] C. Colosqui and A. Oberai. Generalized Smagorinsky model in physical space. *Submitted*, 2007.

[14] J. Domaradzki, K. Loh, and P. Yee. Large eddy simulations using the subgrid-scale estimation model and truncated Navier-Stokes dynamics. *Theoret. Comput. Fluid Dynamics*, 15:421–450, 2002.

[15] A. Dunca, V. John, and W. Layton. *The commutation error of the space averaged Navier-Stokes equations on a bounded domain in Contributions to Current Challenges in Mathematical Fluid Mechanics, Advances in Mathematical Fluid Mechanics, G.P. Galdi and J.G. Heywood and R. Rannacher (Eds.)*, pages 53–78. Birkhauser Verlag Basel, 2004.

[16] C. Foias, O. Manley, R. Rosa, and R. Temam. *Navier-Stokes equations and turbulence*. Encyclopedia of Mathematics and its Applications. Cambridge University Press, 2001.

[17] M. Germano. Differential filters for the large eddy simulation of turbulent flows. *Phys. Fluids*, 29(6):1755–1757, 1986.

[18] M. Germano. Differential filters of elliptic type. *Phys. Fluids*, 29(6):1757–1758, 1986.

[19] S. Ghosal. An analysis of numerical errors in large-eddy simulations of turbulence. *J. Comput. Phys.*, 125:187–206, 1996.

[20] S. Ghosal and P. Moin. The basic equations of the large eddy simulation of turbulent flows in complex geometry. *J. Comput. Phys.*, 118:24–37, 1995.

[21] O. Guasch. *Computational aeroacoustics and turbulence modelling of low speed flows using sub-grid scale stabilised finite element methods*. PhD thesis, Facultat de Matemàtiques i Estadística, Universitat Politècnica de Catalunya, Barcelona, 2007.

[22] J. Guermond. Finite-element-based Faedo-Galerkin weak solutions to the Navier-Stokes equations in the three-dimensional torus are suitable. *J. Math. Pures Appl.*, 85 (3):451–464, 2006.

[23] J. Guermond, J. Oden, and S. Prudhomme. Mathematical perspectives on large eddy simulation models for turbulent flows. *J. Math. Fluid Mech.*, 6 (2):194–248, 2004.

[24] J. Guermond and S. Prudhomme. On the construction of suitable solutions to the Navier-Stokes equations and questions regarding the definition of large eddy simulation. *Physica D*, 207:64–78, 2005.

[25] S. Hickel, N. Adams, and J. Domaradzki. An adaptive local deconvolution method for implicit LES. *J. Comput. Phys.*, 213:413–436, 2006.

[26] J. Hoffman and C. Johnson. A new approach to computational turbulence modeling. *Comput. Methods Appl. Mech. Engrg.*, 195:2865–2880, 2006.

[27] T. Hughes. Multiscale phenomena: Green's function, the Dirichlet-to-Neumann formulation, subgrid scale models, bubbles and the origins of stabilized formulations. *Comput. Methods Appl. Mech. Engrg.*, 127:387–401, 1995.

[28] T. Hughes, V. Calo, and G. Scovazzi. Variational and multiscale methods in turbulence. In *Proc. of the XXI International Congress of Theoretical and Applied Mechanics (IUTAM)*. Kluwer, 2004.

[29] T. Hughes, G. Feijóo, L. Mazzei, and J. Quincy. The variational multiscale method–a paradigm for computational mechanics. *Comput. Methods Appl. Mech. Engrg.*, 166:3–24, 1998.

[30] T. Hughes, L. Mazzei, and K. Jansen. Large eddy simulation and the variational multiscale method. *Comput. Visual. Sci.*, 3:47–59, 2000.

[31] T. Hughes, L. Mazzei, and A. Oberai. Large eddy simulation of turbulent channel flow by the variational multiscale method. *Phys. Fluids*, 13(6):1784–1798, 2001.

[32] T. Hughes, L. Mazzei, and A. Oberai. The multiscale formulation of large eddy simulation: Decay of homogeneous isotropic turbulence. *Phys. Fluids*, 13(2):505–512, 2001.

[33] T. Hughes and G. Sangalli. Variational multiscale analysis: the fine-scale Green's function, projection, optimization, localization and stabilized methods. *SIAM J. Numer. Anal.*, 45(2):539–557, 2007.

[34] V. John. *Large Eddy Simulation of Turbulent Incompressible Flows*. Springer-Verlag, 2004.

[35] B. Knaepen, O. Debliquy, and D. Carati. Large-eddy simulation without filter. *J. Comput. Phys.*, 205:98–107, 2005.

[36] A. Kolmogorov. The local structure of turbulence in incompresible viscous fluids for very large reynolds number. *Dokl. Akad. Nauk. SSSR*, 30:299–330, 1941.

[37] L. Lencina, P. Mueller, E. Dari, and G. Buscaglia. Stabilized finite elements in the simulation of homogeneous isotropic turbulence. In *Proc. VIII Congreso Argentino de Mecánica Computacional. Mecánica Computacional*, volume 24, page 142, Buenos Aires, Argentina, November 2005. Ed. A. Larreteguy.

[38] A. Leonard. Energy cascade in large eddy simulation of turbulent fluid flows. *Adv. Geophys.*, 618:237–248, 1974.

[39] M. Lesieur. *Turbulence in fluids*. 3d Edition. Kluwer Academic Publishers, 1997.

[40] D. Lilly. The representation of small-scale turbulence theory in numerical simulation experiments. In H. Goldstine, editor, *Proc. IBM Scientific Computing Symp. on Environmental Sciences*, 1967.

[41] A. Monin and A. Yaglom. *Statistical Fluid Mechanics: Mechanics of Turbulence. Volume II*. Cambridge, MA: MIT Press., 1975.

[42] S. Pope. *Turbulent Flows*. Cambridge University Press, 2000.

[43] P. Sagaut. *Large Eddy Simulation for Incompressible Flows*. Scientific Computing, Springer, 2001.

[44] P. Sampaio, P. Hallak, A. Coutinho, and M. Pfeil. A stabilized finite element procedure for turbulent fluid-structure interaction using adaptive time-space refinement. *Int. J. Numer. Meth. Fluids*, 44:673–693, 2004.

[45] J. Smagorinsky. General circulation experiments with the primitive equations. I: The basic experiment. *Mon. Weather Rev.*, 91(3):99–164, 1963.

[46] A. Tejada-Martínez and K. Jansen. Spatial test filters for dynamic model large-eddy simulation with finite elements. *Commun. Numer. Meth. Engrg.*, 19 (3):205–213, 2003.

[47] O. Vasilyev, T. Lund, and P. Moin. A general class of commutative filters for LES in complex geometries. *J. Comput. Phys.*, 146:82–104, 1998.